Addis Ababa University

Collage of Technology and Built Environment

African Railway Centre of Excellence

The Effect of Track Irregularity on the Underframe Car Body Structure in Light Rail Vehicles

A Research report Submitted to the School of Graduate Studies of Addis Ababa University in Partial Fulfilment of the Requirements for the Degree of Masters of Science in Railway Engineering (Rolling stock)

Prepared By: Yalemtsehay Alebachew (GSR/3482/14)

Advisor: Araya Abera (PhD)

March 2026

Addis Ababa, Ethiopia

APPROVAL

Yalemtsehay Alebachew, a candidate for the degree of Master of Science in Railway Engineering (Rolling Stock), has submitted a thesis titled **"The Effect of Track Irregularity on the Underframe Car Body Structure in Light Rail Vehicles."** The undersigned has examined the thesis and certifies that it is worthy of acceptance.

______________________	____________	______________
Advısor	Sıgnature	Date
______________________	____________	______________
Internal Examiner	Sıgnature	Date
______________________	____________	______________
External Examiner	Sıgnature	Date
______________________	____________	______________
Chairperson(Head of ARCE)	Sıgnature	Date

DECLARATION

I hereby declare that the research project titled "The Effect of Track Irregularity on the Underframe Car Body Structure in Light Rail Vehicles" is completely my original work and has not been summited for assessment to any other institution. All materials from other sources are properly acknowledged.

Yalemtsehay Alebachew

March 2026

ACKNOWLEDGEMENT

To begin with, I would like to thank God for blessing me with the patience and endurance to complete this research, which took longer than I had expected.

I would like to express my sincere gratitude to my advisor, Dr. Araya Abera, for his guidance, support, and valuable feedback throughout the research process. I would also like to extend my appreciation to the staff members of AA-LRT, especially Engineer Henok, Mr. Dula, and Mr. Berhanu, for their generous assistance in providing the necessary data required to conduct this research. Additionally, I would like to thank the staff of the African Railway Centre of Excellence (ARCE), particularly Mr. Biniyam Ayale, for their support and cooperation during this study.

Lastly, I want to sincerely thank my family and friends for their unwavering support, inspiration, and encouragement during my academic career and the completion of my research project. Their support and understanding were crucial in enabling me to finish my project effectively.

ABSTRACT

This study investigates the effect of track irregularities on the dynamic behaviour and fatigue life of light rail vehicle underframes. This was done by a combination of multibody dynamics simulation (MBDS) and finite element analysis (FEA). A 3D underframe geometry model was developed in SOLIDWORKS and integrated as a flexible body to a multibody system dynamic model in SIMPACK to simulate load time histories for various speed conditions. Stresses were analysed using FEA with a quasi-static stress method, and fatigue life was evaluated in ANSYS nCode Design Life. Results show that motor car underframes experience higher vertical and lateral accelerations than trailer car underframes, with effects intensifying at higher speeds. FEM analysis indicates that track irregularities have a significant effect at higher vehicle speeds, thus reducing underframe fatigue life. At 70 km/h, fatigue life reduces to $1.36e^5$ cycles for motor cars and $7.76e^5$ cycles for trailer car underframes, both lower than standard design life. The fatigue life results were validated using the Smith-Watson-Topper (SWT) fatigue life approach and found to be in good agreement. This study provides key findings for improving underframe durability and maintenance practices in urban transit systems.

Keywords: Track Irregularity, Underframe Structure, Light Rail Vehicles, Fatigue Life, Multibody Dynamics, Finite Element Analysis, SWT Approach.

TABLE OF CONTENT

LIST OF FIGURES

LIST OF TABLES

LIST OF ACRONYMS

AA-LRT	Addis Ababa Light Rail Transit
ERC	Ethiopian Railway Corporation
LRV	Light Rail Vehicle
HSR	High Speed Rail
PTC	Positive Train Control
ETCS	European Train Control System
MBS	Multibody System
FE	Finite Element
FEM	Finite Element Method
UIC	International Union of Railway
EN	European Standard
WP	Wireless Power
OCS	Overhead Catenary Systems
EMU	Electric Multiple Unit
U/F	Underframe
LVDT	Linear Variable Differential Transformer
TRV	Track Recording Vehicles
TRC	Track Recording Cars
LVDTs	Linear Variable Differential Transforms
PSD	Power Spectral Density
VTI	Vehicle - Track Interaction
RCL	Riding Comfort Level
RMS	Root Mean Square
SWT	Smith-Watson-Topper
CNR	Changchun Railway Vehicles
FBI	Flexible Body Interface
SIC	Stress Influence Coefficient

LIST OF SYMBOLES

λ: Wavelength

MC1: Motor Car 1

MC2: Motor Car 2

TP: Trailer Car

Zt: Track Irregularity

C1: Damping 1

C2: Damping 2

K1: Stiffness 1

K2: Stiffness 2

V: Speed

M: Mass

MW1: Mass of wheelset 1

MW2: Mass of wheelset2

L1: Longitudinal distance from centre of gravity to wheelset 1

L2: Longitudinal distance from centre of gravity to wheelset 2

J: Mass inertia moment

$\varepsilon f'$: Fatigue coefficient of ductility

$\sigma f'$: Fatigue coefficient of strength

c: Fatigue exponent of ductility

b: Fatigue strength exponent

σmax: Maximum stress

$\Delta\varepsilon/2$: Strain amplitude

Nf: Fatigue life cycles

E: Modulus of elasticity

CHAPTER 1- INTRODUCTION

1.1 Background

The railway transportation system is the basis of modern mass transit. It provides high-capacity travel, operational efficiency, and lower environmental impacts than other forms of transportation. It is considered the most economical and energy-efficient form of transportation in the world, second only to water transportation[1][2].

Urban transit systems supply the transportation needs of densely populated cities. These systems offer high-capacity transportation for urban population to decrease traffic congestion. [3][4]. Compared to road transportation, urban transit systems reduce greenhouse emissions, increase air quality, and they are also more environmentally friendly. Metro and light rail vehicles (LRVs) are widely used rail vehicles in urban transit systems [5].

1.1.1 Light Rail Vehicles

Light rail vehicles (LRVs) are a form of urban rail transit commonly used for urban public transportation. They are lightweight rail vehicles running on specially designed tracks. LRVs are designed for medium-capacity urban transportation. These vehicles can travel in various environments, such as on-street, they share the street with automobiles and pedestrians, semi-exclusive, or entirely exclusive tracks [6][4]. These vehicles operate at lower speeds than standard conventional trains, since they make more frequent stops. They are powered by overhead electrical lines [7][3].

LRVs are commonly used for city transport for several reasons. First, they are lightweight vehicles that can stop faster. Therefore, they are ideal for cities with a large number of stops. Secondly, LRVs use the same roadways as cars, buses, and pedestrians [3]. Furthermore, the low floor design of the vehicles allows easy passenger boarding.

LRVs are advancing their power supply system from overhead electrical lines to hidden rails and wireless power (WP) technology. These advancements increase urban aesthetics and also significantly decrease maintenance needs [4][7].

Based on a percentage of low floor height, Light Rail Vehicles are divided into two groups: trains with 70% and 100% low floor height.

100% Low-Floor LRVs: These vehicles have a completely low-floor structure that is between 300 and 350 mm above the rail. The design of the vehicle increases accessibility and makes it easier for all categories of passengers, including those in wheelchairs, to board and move inside the train [8].

70% Low-Floor LRVs: In these vehicles around 70% of the floor area is low, which is about 350 mm above the rail. The remaining 30% of the floor is elevated to shelter the mechanical and electrical parts of the vehicle [8].

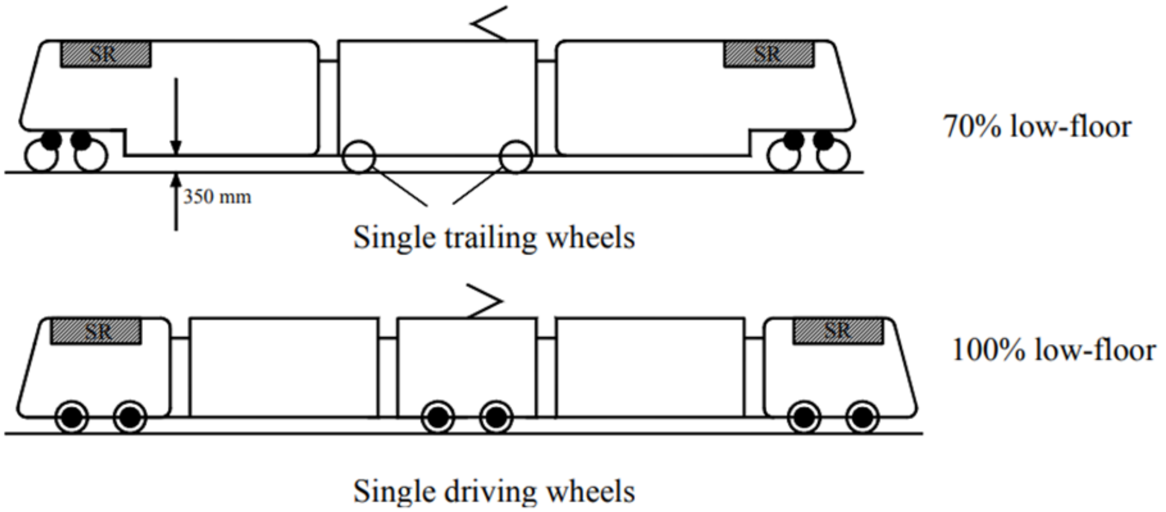

Figure 1.1 70% and 100% low floor LRVs [8]

One of the critical components of a rail vehicle is the underframe car body structure. It is the basic framework in which the car body is built [9]. It supports the train's main body and gives it structural integrity [10], [11]. Underframe supports vehicle weight, the vertical load from the passengers, and the traction and braking forces. Furthermore, underframe also used to mount electrical and mechanical equipment’s such as, traction converters, traction transformers, and pantograph compressors [12]. The structural integrity of the underframe is directly related to the vehicle's overall safety, ride comfort and service life [13]. Therefore, the structural strength of the underframe is essential requirement for railway vehicle operation.

There are various factors that influence the structural strength of the rail vehicle underframe, such as passenger overloading, vehicle operating speed, track irregularities, traction and braking forces, and suspension characteristics [14]. However, among these factors, track irregularities are the most critical. Track irregularities are the deviations from the actual track geometry [15]. These track deviations can be caused by traffic density, maintenance practices, operating speed, and environmental conditions.

The major source of external excitation in a rail vehicle underframe is track irregularities. They produce continuous vibration and dynamic forces on the underframe structure while the vehicle is in motion [16], [17], [18]. When the vehicle runs on an irregular track, vibrations and dynamic forces from the vertical and lateral irregularities are transferred to the vehicle's car body and underframe. As a result, the underframe will experience cyclic loads, which accelerate the fatigue damage of the structure. Therefore, track irregularity is chosen as the main subject of this study since it is the critical factor affecting the structural response and fatigue life of railway vehicles' underframes.

The main goal of this study is to investigate the effect of track irregularity on the dynamic behavior and fatigue life of the underframe structure of light rail vehicles by using the Finite Element Method (FEM) and Multibody Dynamic Simulation (MBDS).

1.2 Statement of the Problem

Track irregularities are the major causes of external excitations in railway vehicles [19]. These excitations, induced by uneven tracks, increase vibration and also apply cyclic stress on the vehicle components. The stress accelerates the fatigue damage of the vehicle components [20], [21].

The underframe is the primary structure that runs the whole length of the train and bears the weight of the vehicle, mechanical and electrical systems, and the interior furniture [22][10]. When a train runs over an uneven track, the irregular track geometry induces vibration and stress in the underframe structure. This dynamic load gradually causes fatigue damage and reduces the service life of the underframe. Consequently, it will result in increased maintenance needs, higher operational costs, and compromised light rail service efficiency and reliability.

Numerous studies have examined the influence of track defects on the rail vehicle dynamics and fatigue damage of components. However, most of these researches have been done on high-speed rail (HSR) systems, and the results of their investigation cannot be applicable to light rail cars because of the differences in axle loads, operating speeds, track conditions, and maintenance practices. Furthermore, limited researches have been conducted on the effect of track irregularities on the dynamic performance and fatigue life of the LRV underframe.

Therefore, extensive research is required to examine the effect of track irregularities on the dynamic response and fatigue life of LRV underframe. This research will investigate the effect of track irregularities on the LRV underframe structure by analysing its dynamic responses under different operating speed conditions and also predicting its fatigue life, using multibody dynamic simulation (MBDS) and finite element method (FEM).

The findings of this research will demonstrate the critical effect of track irregularities on the fatigue life of underframe, and also provide operational and maintenance guidelines to increase the service life of the underframe.

1.3 Research questions

1. How does the underframe structure respond dynamically to the excitations from track irregularities at various operational speeds?
2. What is the estimated fatigue life of the underframe at the maximum vehicle speed?
3. In which parts of the underframe are the stress concentration nodes (hotspots) located?

1.4 Objective of the Study

1.4.1 1.4.1 General objective

The main purpose of this study is to investigate the effects of track irregularities on the dynamic behavior and fatigue life of the underframe structure of light rail vehicles.

1.4.2 Specific objectives

1. Analyze the dynamic behavior of the underframe due to the track irregularity excitation at various vehicle operating speeds.
2. Predict the fatigue life of the underframe at various vehicle operating speeds.
3. Locate the stress concentration nodes (hotspots) in the underframe.

1.5 Scope and Limitation of the Study

This study utilized a multibody dynamic simulation (MBDS) to investigate the influence of irregular track geometry on the dynamic performance of LRVs underframe. The actual vehicle and underframe data were collected from the AA-LRT rolling stock depot. However, the study was forced to manually measure the dimensions of the underframe due to the lack of available design documents. Furthermore, due to the lack of complete measured track data from the AA-LRT, track geometry data for the MBDS was collected from the Chinese urban rail transit system. These data were selected because both transit systems follow similar Chinese railway standards and exhibit comparable moderate levels of track irregularities.

The study is limited to only 70% low-floor light rail vehicles, which may restrict the ability to generalize results to other vehicle designs. Other affecting parameters, such as curved track geometry, passenger load variations, and environmental conditions, were not considered in this research to avoid computational complexity. These factors are therefore recommended to be addressed in future studies to provide a provide a better evaluation of the performance of an underframe under realistic operating conditions.

1.6 Significance of the Study

The significance of this research is to show the influence of track irregularities on the structural integrity of the light rail vehicles (LRVs) underframe structure. Existing research has mainly focused on investigating the effect of random dynamic loads on high-speed trains and their components. However, this research examines the dynamic behaviour, fatigue life, and stress concentration areas in the LRV underframe when the vehicle is exposed to track irregularity excitation at different vehicle speeds.

The findings of this research will bridge the knowledge gap on the effects of track irregularities on the dynamic behaviour and fatigue life of LRV underframes. It also provides insights that support maintenance planning to prevent fatigue induced failures and enhance vehicle safety, reliability, and service life.

1.7 Organization of the Study

This study is structured into five chapters.

Chapter One: Introduction presents background information on railway transportation and light rail vehicles. It also includes the problem statement, research questions, objectives, scope and limitations, significance of the study, and organization of the study.

Chapter Two: Literature Review discuss previous research relevant to this study. It identifies gaps in the existing literature and explains how this study aims to address them.

Chapter Three: Methodology explains the research approach and provides detailed information on the simulation procedure.

Chapter Four: presents the simulation results and discuss the influence of track irregularities on the underframe dynamic behaviour and fatigue life.

Chapter Five: conclude the main findings of the study, highlights its contributions, and provides recommendations for future research directions.

CHAPTER 2 - LITERATURE REVIEW

2.1 Introduction

This literature review discusses the previous studies from different research works that have been carried out on the effect of track geometric defects on rail vehicles car body structure, vehicle-track interaction dynamics, vibration response of the underframe, and fatigue life of the underframe. Numerous researchers have investigated the impact of track geometry faults on the vehicle car body structure of both passenger and freight trains using dynamic simulations, computational analyses, and experimental methods.

In this section, the literature review discusses the approaches that have been used by different scholars, points out the gaps in their findings, and presents some of the recommended solutions proposed by different academics in the subject. Each of these topics is reviewed in a structured and detailed way to determine the research gap that needs to be addressed in this study to accomplish the stated research goals.

To conduct this review, prominent scientific journals such as, Scopus, ScienceDirect, Google Scholar, Directory of Open Access Journals (DOAJ), Taylor and Francis are used to find related researches. This procedure ensures that the review is built on reliable and high-quality sources, providing a strong basis for the current study.

2.2 Railway Track

Railway lines are built to allow trains to transport people and cargo over long distances. These track structures are expected to guide and facilitate the safe, comfortable, and cost-effective movement of any rolling stock through them [23]. They are designed to handle both static and dynamic forces from the trains.

Track components are generally divided into two main groups: the superstructure and the substructure [24]. The superstructure includes visible components of the track such as rails, rail pads, concrete sleepers, and fastening systems (bolts, nuts and clips), while the substructure includes geotechnical components such as sub-ballast, ballast, and subgrade [25]. Both the superstructure and substructure play a critical role to ensure the safety of passengers during their journey and the smooth running of freight trains.

Steel rails are longitudinal steel components placed on evenly spaced sleepers. They are considered the most important part of the track. They guide the wheels of the rail vehicle, and they are stiff enough to bear the weight of the trains running on them. Primarily, these rails carry and transfer the loads to the sleepers below them. Furthermore, in modern electrified lines, they are used to conduct electrical signals for the trains [26].

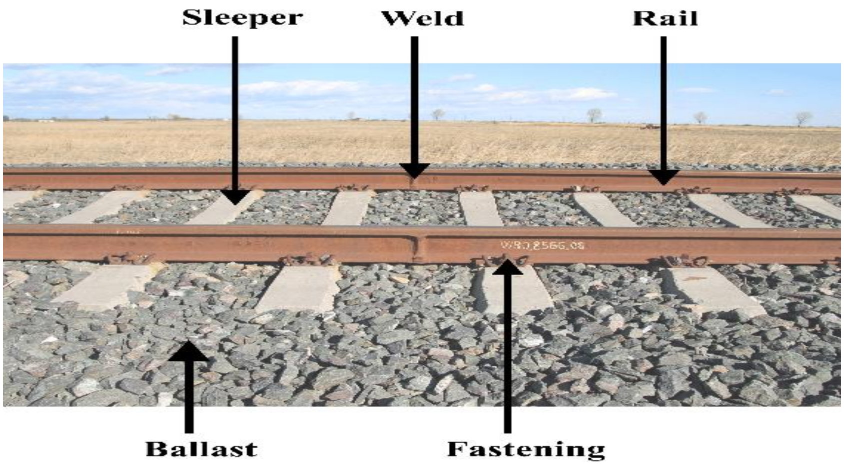

Figure 2.1 Railway track [27]

2.3 Track Irregularity

Track design comprises horizontal and vertical curvature, track gauge, and cant to adjust train stability and safe operation [28]. Variations to this design geometry are caused by the condition of the superstructure and substructure elements. In addition, factors such as traffic density, operating speeds, axle loads, environmental conditions, and maintenance practices also play a significant role. Gradually, because of the repetitive traffic loads, rail wear, settlement, and other reasons, the running track deviates from its designed profile [24][29]. These deviations from the intended geometry are referred to as track irregularities [28].

Track irregularities are categorized into five main types based on EN 13848-1 [30][29] as shown in Figure 2.2 and explained below.

- **Longitudinal level irregularities**: are deviations in the vertical direction of railway track geometry [31].
- **Alignment irregularities**: are deviations in the lateral direction of railway track geometry [24].

- **Cant irregularities (cross level irregularities)**: the difference in elevation between the left and right rails [32].
- **Gauge irregularities:** are the deviation in the distance between inside of the left and right rails, usually measured 14 mm below the running surface[31].
- **Twist:** the difference between two cants taken at defined distance apart, usually expressed as gradient between the two points of measurement [32].

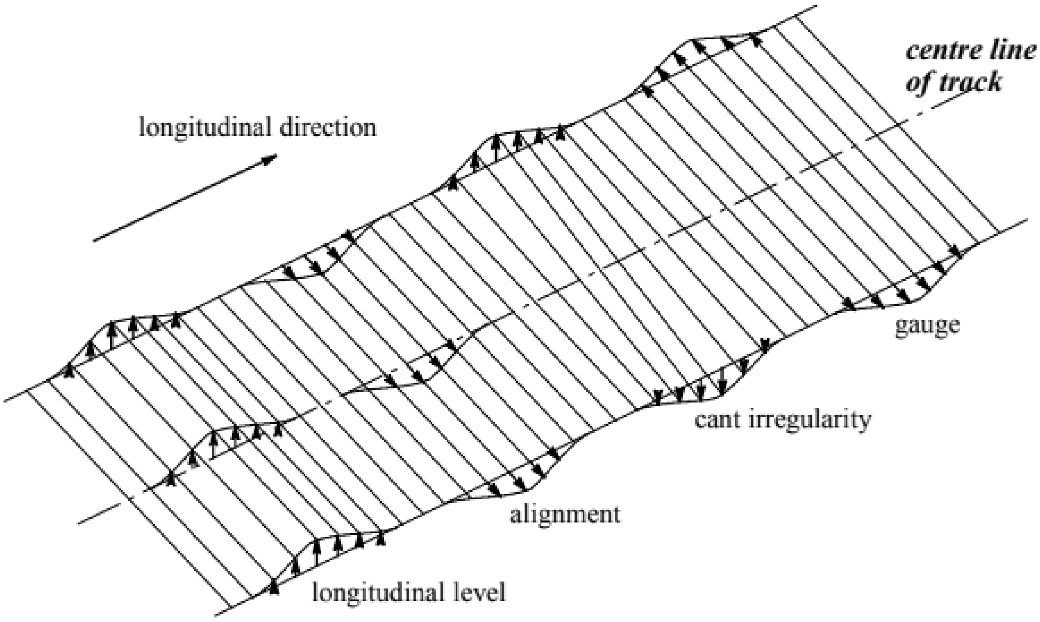

Figure 2.3 Types of track irregularities [20]

Based on their wavelength (λ) track irregularities are also classified into two types [33] [28].

- **Long-wavelength irregularities**: have a wavelength greater than one meter ($\lambda > 1$ m) and result from track settlement, sleeper spacing, track geometry variations, and, in some cases, wheel out-of-roundness [34].
- **Short wavelength irregularities:** have a wavelength less than one meter ($\lambda < 1$ m) and can be caused by factors such as rail corrugation, track stiffness variations, and wheel polygonazation [26].

To measure track irregularities in railway tracks, different types of machines and vehicles are used, generally called track-recording vehicles (TRV) or cars (TRC) [35]. TRVs measure the track geometry and irregularity as they go over the track using an acquisition system made up of accelerometers, linear variable differntial transforms (LVDTs), lasers, and cameras [36].Track geometry trolleys are another commonly used technique where instrumentation is installed on a trolley. A recent technique that is becoming more common is mounting accelerometers on the axle boxes, bogie frames, and carbodies to measure track irregularities [28][30].

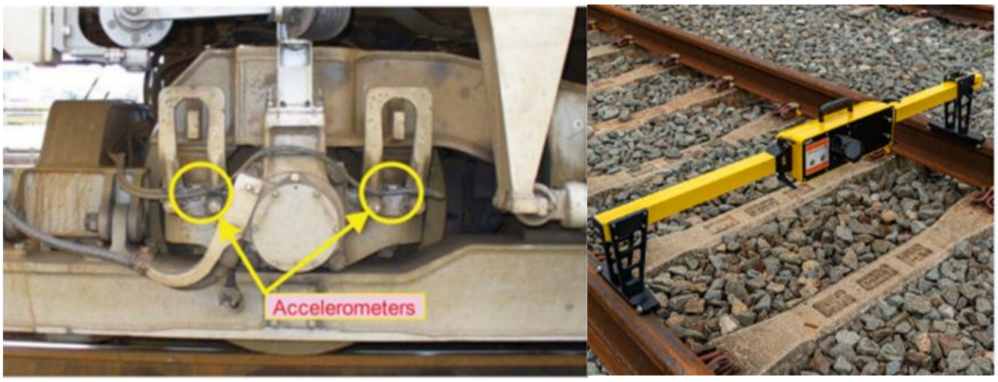

(a) (b)

Figure 2.4 Track geometry trolly and Axle box accelerometer [37]

2.4 Vehicle - Track Interaction

Vehicle-track interaction (VTI) is the dynamic interaction between a moving vehicle and the track over which they operate. This dynamic interaction is critical in the design and operation, performance, safety, and maintenance needs for both the vehicle and the track structure [35].

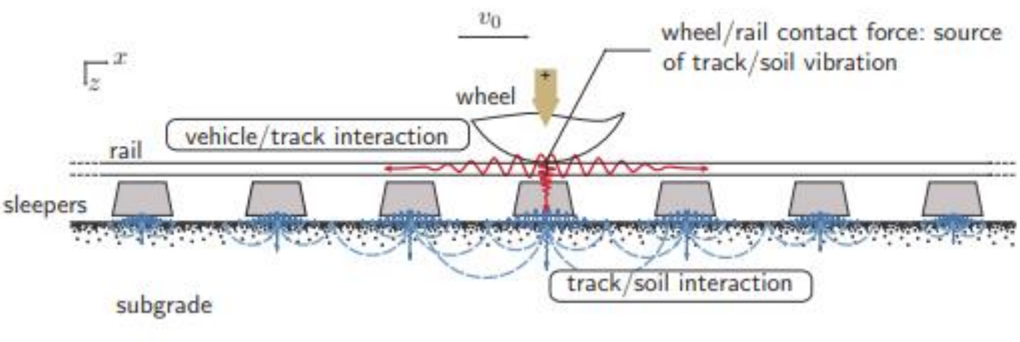

Figure 2.5 Vehicle – track dynamics [38]

The railway vehicle system is vulnerable to excitation from various sources. These include track defects, rail corrugations, wheel defects like polygonization, turnouts and joints, and variations in track flexibility [39]. Track defects and variations in track flexibility generate continuous, random vibrations (stochastic excitation) in the track-vehicle system, while turnouts and joints cause temporary disturbances (transient behaviour) [40]. Wheel out-of-roundness, on the other hand, is a self-induced source of strong, high-frequency vibrations, arising from imperfections on the wheels themselves [30].

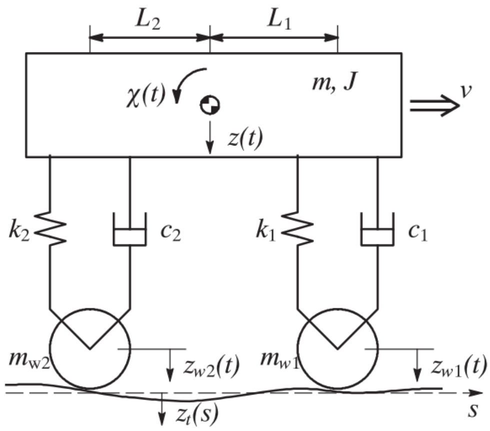

Figure 2.6 2- DOF model moving along rigid track with track irregularities zt present [30].

For safe and comfortable train journeys at various speeds, a railway track structure must be precisely levelled and aligned. Any irregularities can cause the train to undergo excessive lateral and vertical movements[19]. These oscillations initiate a series of negative effects. Passengers experience discomfort due to the vibration, and vehicle and track components are damaged. Severe irregularities may threaten the overall safety of the vehicle operation [29], [41].

2.5 Influence of Track Irregularities on Rail Vehicle Dynamics

Track irregularities such as rail joints, track unevenness, and track stiffness variations have a significant influence on the rail vehicle dynamics, including ride quality and vehicle safety. [29][42]. Vehicle dynamic responses from these irregularities can be measured directly by accelerometers or indirectly using strain gauges on the wheelset [31], [43].

These are the most common parameters measured on the rail vehicles to show their response to the track conditions [30]:

- **Wheel-rail forces:** measured by strain gauges mounted on wheelsets. These dynamic vertical and lateral forces are usually caused by track irregularities, corrugations, and track stiffness changes and are associated with safety [44]. Tracks with large irregularities will lead to high dynamic forces between wheel and rail, which might cause increased wear and track and rail component failures [35].
- **Accelerations**: Vibrations are measured using accelerometers placed on bogie frames, axle box and the car body [34], [37]. Bogie frame and axle box accelerations are more safety-related, while car body accelerations primarily impact ride comfort.
- **Movement between suspension steps**: Excessive movement between suspensions can pose a safety risk [31].

Different types of track irregularities have different effects on rail vehicle components and their dynamic performance [45]. Longitudinal level irregularities, also known as vertical irregularities, can cause the vehicle to pitch and bounce[42]. On the other hand, alignment irregularities (lateral irregularities) and gauge irregularities induce significant lateral forces on the vehicle wheels, and under severe conditions, they can also lead to derailment. Derailment is a catastrophic accident in train operations. It happens when the vehicle movement causes the wheels to leave the track [35]. Derailment occurs due to several reasons, one of the most common cause is flange climbing [29]. Another cause is cross-level irregularity, which has a strong influence on the vehicle's lateral behaviour, increasing the derailment coefficient [46]

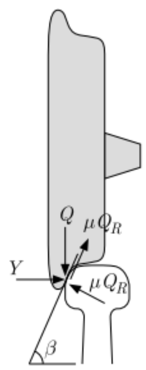

Figure 2.7 Lateral and vertical force at contact patch [47]

The derailment coefficient is a critical indicator of potential derailment and is determined by the ratio of lateral to vertical forces acting on the wheel [29].

$$\text{Derailment coefficient} = \frac{Y}{Q} = \frac{L}{V} = \frac{\tan\delta - \mu}{1 + \mu tan\delta} \tag{2.1}$$

Where, Y (L) = lateral force, Q (V) = vertical force, μ= friction coefficient, δ= flange angle, and β = contact angle of the rail and wheel flange [29] .

To prevent wheel climbing during train operation, the derailment coefficient must not be greater than 0.8 [29].

2.5.1 Dynamic Effects of Short and Long-Wavelength Track Irregularities

Track irregularities wavelength has a critical effect on the dynamic response of railway trains [29]. The influence of short-wavelength irregularities is very different from that of long-wavelength ones. Short wavelength irregularity (railhead corrugations) presents a greater safety risk by increasing the derailing coefficient [42]. In addition, they generate unwanted noise and vibration. On the contrary, long-wavelength irregularities mainly have effects on ride comfort, vehicle stability, and induce low-frequency oscillations in trains [29][48]. Since a typical train's natural frequency is around 1 Hz, the resonance caused by long wavelengths increases the oscillations. Then, it finally reduces the RCL (ride comfort level) [33]. Moreover, it is the short-wavelength irregularities that mostly affect vehicle performance, although the long-wavelength ones are very significant regarding lateral forces and accelerations [49].

Haigermoser et al. [34] explored the influence of track irregularities of long wavelength on the high-speed vehicle vibration levels through field tests and 3D finite element analysis. Car body vibrations were largely influenced by long-wavelength irregularities. Similarly, Hung et al. [33] used a numerical vehicle-track system dynamics model (VTSDM) to understand the dynamic responses of high-speed trains to long-wavelength track irregularities. The results indicate that there is a strong correlation between train speed and natural frequency with long-wavelength irregularity. A study by Karis et al.[29] showed that longitudinal level irregularities, particularly at long wavelengths, have a strong influence on vertical body acceleration, which is related to ride comfort.

Song et al. [50] investigated the effect of short-wavelength track irregularity excitation on the dynamic response of the EMU car body underframe using a rigid-flexible vehicle model.

The accelerations on the concerned locations of the underframe were measured while the EMU was in service. The centre of the underframe selected to compare simulation results with the experimental result from the test line. The test line results revealed that the dominant frequency is 30 Hz and no low frequencies (below 10Hz) present. Song et al. [50]concluded that experimental and simulation compression results showed that rigid – flexible coupled model accurately simulate high frequency vibration of car body.

2.5.2. Longitudinal and Alignment Irregularity

Longitudinal irregularities are caused by rail contraction and expansion due to temperature change (thermal forces), train braking system forces and acceleration, ballast settlement, and ballast crushing [45]. These geometric defects can cause a car body to pitch and bounce; these exert strong wheel-rail vertical force, increase vehicle components damage, and reduce ride comfort [42]. On the other hand, track alignment can cause a vehicle to sway and yaw, producing significant lateral wheel and axle forces that impact ride comfort, running safety, and fatigue damage to the vehicle and track components. Cross-level irregularities are another frequent geometric defect in tracks that can lead to a car body rolling and swaying [29].

2.6 Underframe Car Body Structure

The underframe, also known as the chassis, is the fundamental structure on which the car body is built. It provides structural integrity and support for the train's main body, allowing it to withstand the forces and vibrations experienced during operation[51][52]. It is the primary structure that runs the whole length of the train and bears the weight of the train, mechanical and electrical systems, and the interior furniture [22]. The structure is designed to support the vehicle’s weight, and vertical load from the passengers, the traction and braking forces, the horizontal load transmitted through the coupler, and the dynamic load transferred by the bogie [53].

Figure 2.8 AA-LRT vehicles underframe structures

The structure and part of the underframe are not the same for both passenger and freight trains. For example, the underframe in passenger trains may incorporate passenger door openings and gangway openings in the end walls for easy access and mobility, whereas in freight trains, underframes are specifically designed to accommodate the cargo to be carried. Passenger train underframes may take many different forms depending on the train type and purpose; for instance, High-speed trains have underframes designed for stability at high speeds. These structures are often lighter and more aerodynamic, incorporating advanced materials like aluminium alloys to minimize weight while maintaining strength [54]. In contrast, LRVs (Light rail vehicles) have underframes specially designed to handle the unique operational demands of urban transit systems. This structure of LRVs needs to be strong enough to support the frequent stopping and starting, and weight from the passengers. Some of the most common structural components in conventional passenger rail vehicle underframes include centre sill, side sill (side beam), end beam, bolster, cross bearers, cross beam, and traction beam, and an end buffer beam [55][51][56][57].

- **Centre sill**: - forms the foundation of the chassis and extends longitudinally through the centre of the car. It transfers the majority of buff and draft forces through the vehicle [58].
- **Side sill**: - are longitudinal members, which extend the whole length of the car body on both side of the vehicle [59].
- **Bolster**: - is across member used to transfer lateral and vertical loads forces from the car body to the bogie and support the traction motor [57].
- **Cross bearers**: - are lateral members that joins centre sill to side sill and assist in distributing the weight among the car's longitudinal members [60].
- **Cross beams**: - mostly used to suspend various equipment beneath the vehicle body.
- **Traction beam**: - are mostly encounters vertical compression forces and also subjected to significant bending moment.
- **End buffer beam**: - is mostly utilized for the car body's end connectors.

Together, these parts form a system that helps keep a vehicle's structural integrity and camber.[57].

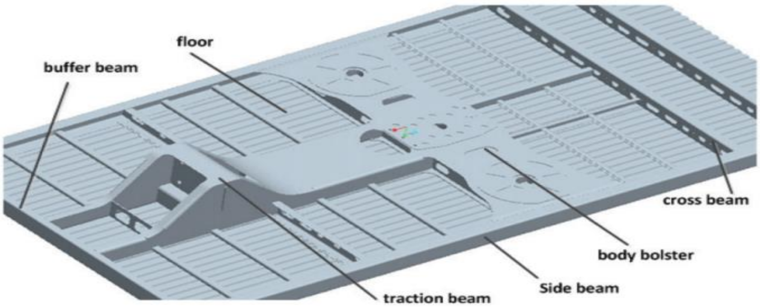

Figure 2.9 Underframe of Electric multiple unit [52]

Steel is commonly used for the chassis structure, mostly low-alloyed steel with a small number of alloying elements like chromium, molybdenum, or nickel. These alloying elements improve the strength, toughness, and durability of the steel. Besides, some modern high-speed trains use aluminium alloys for the chassis. A7N01P-T4 and Al-Mg-Zn aluminium alloys are widely used due to their light weight and high strength [54].

2.7 The Fatigue Life of rail vehicles Car Body Structure

Fatigue occurs when a material is subjected to cyclic loading over time [61] [62]. In railway vehicles, fatigue life cycle refers to the number of load cycles a rail vehicle can endure before structural failure. Fatigue is a critical design parameter, since the vehicle's car body is the main load-bearing structure [63]. Higher dynamic stress is the principal cause of rail vehicles car body fatigue damage [64]. These excessive dynamic loads result from wheel-rail interaction, track imperfections, breaking, and coupling effects. Such loads increase the car body's natural frequency by producing stress cycles that concentrate in weak areas, such as welded joints, bolted connections, and cut-outs. When the dynamic stresses repeatedly exceed the fatigue strength of the material in these weak areas, cracks start to initiate and gradually propagate [52] [64].This cumulative process leads to visible fatigue damage or even failure if not detected on time.

Table 2.1 Summary of published literatures on the fatigue life of rail vehicle car body structure

SN	Researcher	Year	Research Objective	Methodology	Key Findings	Identified Gaps
[65]	Yaohui Lu, Linyuan Dang	2018	Investigated the dynamic reliability of high-speed train car body under random load.	Using MBDS and FEM	welded areas of the vehicle's body exhibit less fatigue resistance than base metal, making them more prone to failure.	It considers general random loads without varying defect severity.
[66]	Yaohui Lu, WeiBi	2019	Studied the fatigue damage of high-speed train car bodies due to longitudinal loads.	Use theoretical modelling, numerical simulations, and analytical techniques.	The longitudinal load has a significant effect on the fatigue damage of the car body.	Only considers a high-frequency, and small-amplitude excitations.
[67]	Miao, B. R. Zhang, W. H.	2012	Studied the effect of vehicle dynamic behaviour on the car body fatigue damage.	Using MBDS and FEM	The vehicle dynamic behaviour of a vehicle has a significant effect on fatigue property of car body.	Does not calculate the fatigue damage of car body at high-risk areas.
[68]	Bingrong Miaoa, Weihua Zhang	2009	Evaluate the fatigue life of railway vehicle car body structures under random dynamic loads.	Using MBDS and FEM	Predicts the fatigue life of critical nodes in the car body.	It didn't examine the effect of track defects to fatigue damage of car body.
[10]	Wang, Cheng-Qiang	2017	Evaluate the vibration response of an Electric Multiple Unit (EMU) car body underframe.	Using MBDS and FEM	Captures local resonance at 30 Hz in EMU underframe using rigid-flexible model with short wave excitation.	Focuses only on vibration at the centre of the EMU car body underframe.

2.8 Research Gap

In general, based on various studies summarized in Table 2.1 above, even though vast research has investigated the dynamic behaviour and fatigue damage of vehicle car bodies, most of them have focused on high-speed railway vehicles. These studies mainly examine the dynamic behaviour of the entire car body structure, while the underframe, one of the most critical load-carrying components subjected to cyclic stresses during service, has received limited attention. Furthermore, previous studies have generally considered random dynamic loads without specifically analysing the effects of track irregularities on the vehicle's car body.

For light rail vehicles, particularly those operating within urban areas the effect of track geometric defects on underframe dynamic behaviour remains unstudied. The particular operating conditions, maintenance practices, and environmental conditions of LRVs additionally limit the direct generalization of findings from high-speed rail investigations. As a result, there is a wide research gap in the field of the effect of track geometry defects on the light rail vehicles underframe structures at various speed conditions. The current study is hence motivated to investigate the dynamic response and fatigue life of underframe structures under irregular track profiles.

CHAPTER 3 – METHODOLOGY AND MULTIBODY SIMULATION

3.1 Introduction

This research utilized a combined approach of multi-body dynamics (MBD) simulation and finite element analysis (FEA) to predict the fatigue life of a light rail vehicle's underframe car body structure subjected to track irregularity excitation. The entire research process is divided into three major phases.

In the first phase (data collection), input parameters and reference data were collected from the relevant literature and the AA-LRT depot. Comparable research and international standards were also reviewed for validation purposes.

The second phase (modelling) involved developing the vehicle and underframe structural models. A 3D model of the underframe car body structure was created in SOLIDWORK. Then the model was exported to Ansys APDL to generate substructure files (cdb & sub). These files were then converted to flexible body interface (FBI) file format for SIMPACK. Concurrently, the multibody model of a 70% low-floor LRV was developed in the SIMPACK simulation package. The vehicle model consists of three car bodies, front motor car (MC1), trailer car (TP) and rear motor car (MC2), as well as three bogie frames and six-wheel sets, which are regarded as a rigid body. Subsequently, the underframe FBI file was imported as a flexible body in the SIMPACK multibody system.

In the third phase (simulation and fatigue analysis), the dynamic simulations were performed in SIMPACK at three operating speeds using track irregularity data as the excitation input. From the SIMPACK Postprocessor results, the lateral and vertical accelerations experienced by the MC1, TP, and MC2 underframes were extracted and used to calculate force time histories. These loading histories were then applied in ANSYS n-Code Design Life to estimate the fatigue life of the underframe. The results were compared and validated using the Smith-Watson-Topper (SWT) fatigue approach and international standards. The overall research methodology is illustrated in the flowchart presented below.

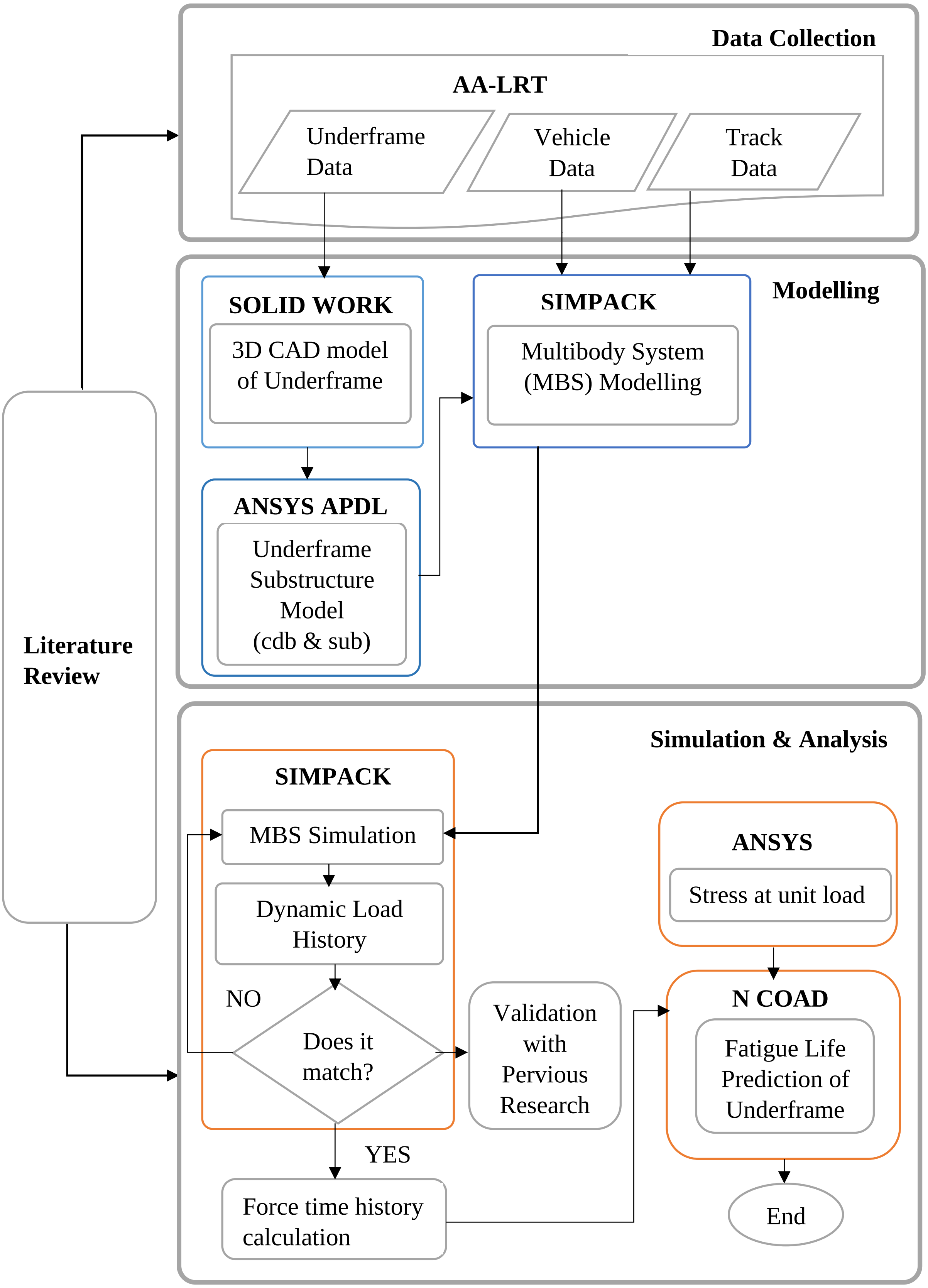

Figure 3.1 Research methodology flowchart

3.2 Data Collection

All the parameters of vehicle data required for multibody dynamic simulation were derived from AA-LRT rolling stock department. For reference and validation purpose related research works were gathered from international standards such as EN and UIC and from published literatures, journals, conference papers.

The collection of track irregularity data from the AA-LRT system presented significant challenges. The available data in the civil infrastructure department, which was obtained through manual measuring systems during track inspection, was incomplete and contained large missing data to use in multibody dynamic simulations conducted in SIMPACK. To achieve robustness and credibility of the study, track irregularity data were instead obtained from the Chinese rail transit [69]. This data was selected as appropriate since both transit systems operate under Chinese standards and present moderate track irregularities, indicating similar track characteristics.

Table 3.1 Track irregularity from China rail transit [69]

Parameters	A	B	C	D	E	F	G
Left rail, vertical	0.127	-2.1531	1.5503	4.9835	1.3891	-0.0327	0.0018
Right rail, vertical	0.3326	-1.3757	0.5497	2.4907	0.4057	0.0858	-0.0014
Left rail, lateral	0.0627	-1.184	0.6773	2.1237	-0.0847	0.034	-0.0005
Right rail, lateral	0.1595	-1.3853	0.6671	2.3331	0.2561	0.0928	-0.0016

3.3 Underframe Structure Design and Material Specifications

In 70% low-floor LRVs, the motor car underframe comprises both the high-floor and the low-floor configuration. The high-floor configuration includes the floor beam, longitudinal beam, side beam, draft sill assembly, and bolster. Meanwhile, the low-floor configuration comprises the lower floor beam, lower cross beam, side beam, end beam, and lower hinge joint seat. The trailer car underframe is similarly composed of the bolster, side beam, end beam, floor beam, and lower hinge joint seat [10].

The underframe structure of AA-LRT vehicles is made of S500MC high-strength carbon steel panels and weathering steel 09CuPCrNi-A [70].

Table 3.2 Mechanical properties of carbon steel panel S500MC [70]

Material	Property					
carbon steel panel S500MC	Density	Tensile strength	Yield strength	Modulus of elasticity	Poisons Ratio	% Elongation
	7880Kg/m3	689Mpa	345Mpa	210pa	0.265	40

Table 3.3 Chemical component of high weathering resistant structure steel [70]

Material Type	Chemical component %							
	C	Si	Mn	P	S	Cu	Cr	Ni
Q345GNHL	≤0.12	0.25 ~0.75	0.20 ~0.50	0.07 ~0.15	≤0.035	0.25 ~0.55	0.30 ~1.25	≤0.65

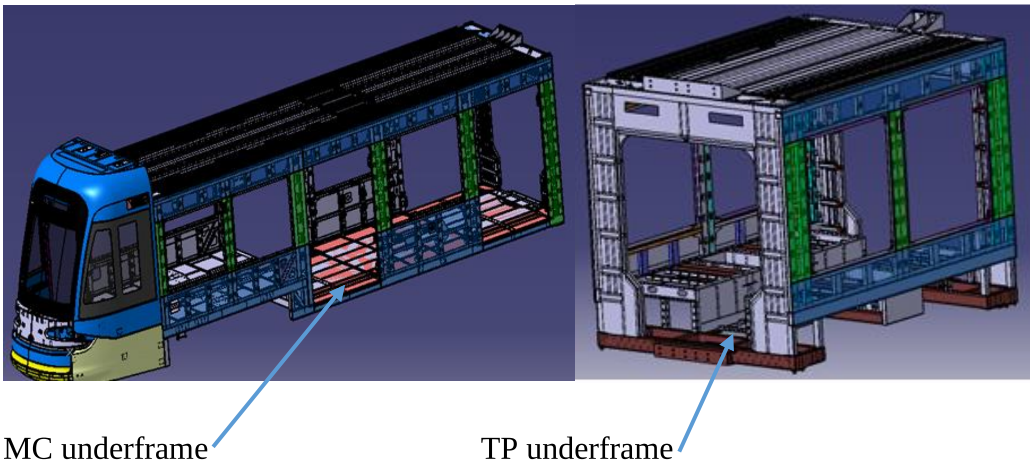

MC underframe TP underframe

Figure 3.2 Motor car and Trailer car underframe in AA-LRT vehicles [70]

3.4 Vehicle and Track Parameters

AA-LRT rolling stock are 70% low-floor light rail vehicles powered by 750V DC. The maximum operating speed of the vehicles is 70km/h [71]. Each train set is composed of three cars: two motored cars (MC) and one trailing car (TP). The car body is mainly constructed by the underframe, roof, side walls, and end walls.

The design strength of these vehicles shall meet EN12663-PIV, and the compressed load is 40 tons. The car body steel structure mainly utilizes SUS301L stainless steel and 6005A-T6 aluminium profile, which are specially used for railway vehicles[70].

Table 3.4 Mechanical properties of SUS301L stainless steel [70]

Material type	Yield strength (N/mm2)	Tensile strength (N/mm2)	Percentage elongation (%)
SUS301L-DLT	>345	>689	>40

Table 3.5 Chemical component of SUS301L stainless steel [70]

Material	C	Si	Mn	P	S	Ni	Cr	Others
SUS301L	<0.03	<1.00	<2.00	0.045	<0.030	6.00~8.00	16.00~18.00	<0.20

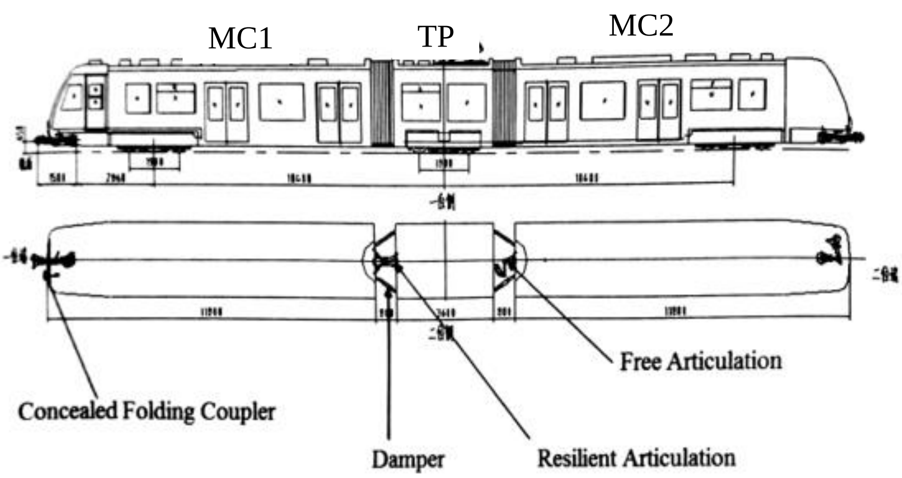

Figure 3.3 AA-LRT Vehicle [70]

To calculate the fatigue damage and simulate the influence of track irregularity on the underframe structure, the following data is required.

Table 3.6 AA-LRT vehicles and Track parameters [70]

Vehicle parameter	Value	Vehicle parameter	Value
Train Total length	28.8m	Wheel set base for motor bogie	1.9m
Motor car body length	12m	Wheel set base for trailer bogie	1.8m
Trailer car body length	3.6m	Wheel set mass	880kg
Height of car body excluding pantograph	3.61m	Wheel set diameter	660m
Height of car from the ground	0.655m	Wheel set moment of inertia x	176kgm^2
Width of car body	2.65m	Wheel set moment of inertia y	70kgm^2
Car body mass (Maximum load)	63000kg	Wheel set moment of inertia z	176kgm^2
Car body mass (Normal load, only sitting)	48000kg	Wheel Profile	S1002
Car body mass (Normal load sitting and standing)	59200kg	Primary spring stiffness along x	7.00E+05N/m^2
Car body mass (no load)	44000kg	Primary spring stiffness along y	7.00E+06N/m^2
Moment of inertia of the car body about x-axis	4375kgm^2	Primary spring stiffness along z	8.00E+05N/m^2
Moment of inertia of the car body about y-axis	8750kgm^2	Primary damping along x	1.53E+05N.S/m
Moment of inertia of the car body about z-axis	8750kgm^2	Primary damping along y	1.53E+05N.S/m
Car body mass (TP)	12325kg	Primary damping along z	1.53E+05N.S/m
Car body moment of inertia about x- axis	3081kgm^2	Secondary spring stiffness along x	0.00E+00N/m^2
Car body moment of inertia about y- axis	6162km^2	Secondary spring stiffness along y	1.65E+07N/m^2
Car body moment of inertia about z- axis	6162km^2	Secondary spring stiffness along z	2.72E+08N/m^2
Bogie mass for motor bogie	5120kg	Secondary damper along x	1.4E+03N.S/m
Bogie mass for trailer bogie	3120kg	Secondary damper along y	4.00E+06N.S/m
Bogie frame mass	985kg	Secondary damper along z	8.00E+06N.S/m
Bogie base distance	10.4m		
Bogie Moment of inertia along x	1250kgm^2	**Track Parameters**	**Value**
Bogie moment of inertia along y	1870kgm^2	Track Profile	UIC 60
Bogie moment of inertia along z	2182kgm^2	Track Gauge	1.435m
MC Underframe Length	12m	Track Length	1000m
TP Underframe Length	3.6	Track Super Elevation	0.1m
Width of Underframe	2.65m	Friction Coefficient	0.4
Lateral wheel position	0.75m	Friction Coefficient	0.4

3.5 Geometric Modelling of Underframe

A three-dimensional model of the motor car (MC) and trailer car (TP) underframe was developed based on technical specifications of AA-LRT using SOLIDWORK 2019. The underframe model includes major structural members, including longitudinal beams, side beams, end beams, and cross beams. For each car, three separate underframes were modelled and assembled into an MC1-TP-MC2 configuration. The 3D models were saved in Parasolid (x.t) file format and exported to ANSYS APDL to generate the substructure model of the underframe to create flexible body interface (FBI) files, and integrate the 3D underframe model into the multibody dynamic system SIMPACK.

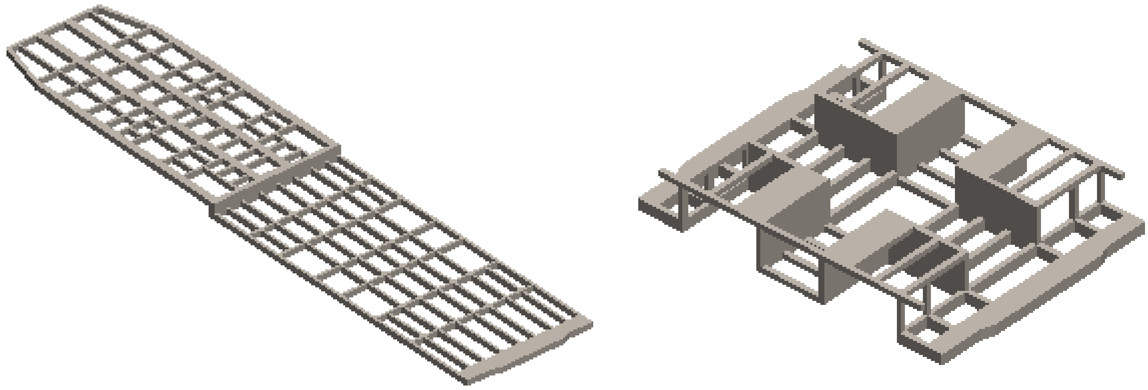

(a) (b)

Figure 3.4 3D CAD model of (a) MC underframe, (b) TP underframe

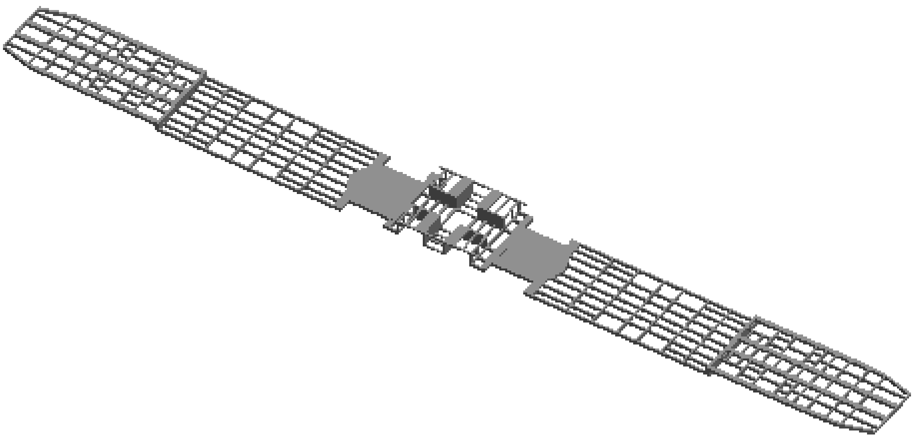

Figure 3.5 Assembled 3D model of train underframe (MC1-TP-MC2)

3.6 Multi-Body Dynamic Model of Vehicle

A Multibody dynamic model of the 70% low-floor LRV was modelled in SIMPACK multibody dynamic software according to the design specifications of the AA-LRT system, as presented in Table 3.6. The model consists of three car bodies: two motor cars and one trailer car, three bogie frames, and six wheelsets, which are connected by force elements and hinge joints. The suspension elements are considered as spring-damper elements. The track was modelled as a straight track 1000m long, and track irregularity has also been imported as an excitation input.

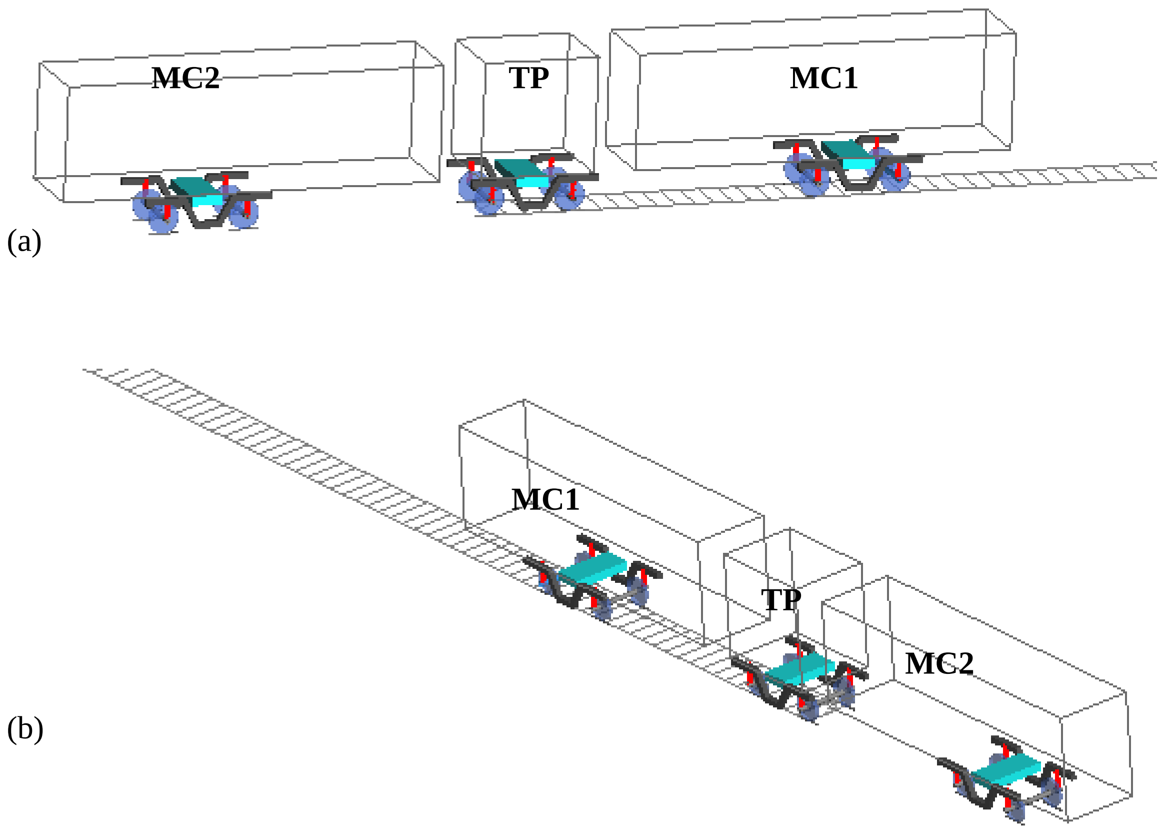

Figure 3.6 (a) Front view, (b) Isometric view of LRV model in SIMPACK.

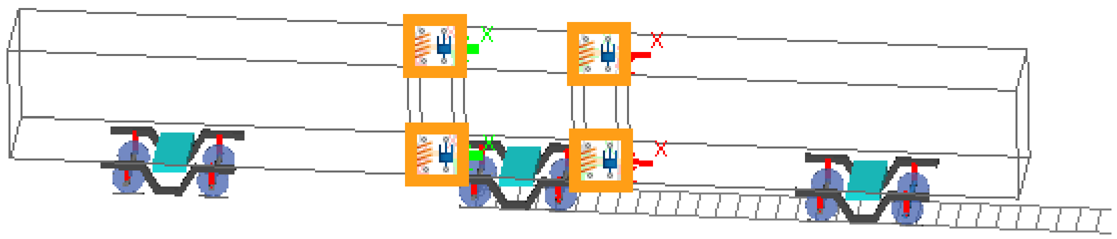

Figure 3.7 Force Elements used between car bodies

To integrate the 3D underframe model into the multibody dynamic system SIMPACK, first, the 3D model was saved in Parasolid (x.t) format and then imported into Ansys APDL. Material properties were assigned, and the structure was discretized using solid 185 elements. After meshing, master nodes were defined in both the MC and TP underframes. The master node links the flexibility with the adjacent multibody system. This master node is defined during the reduction in the FE code by specifically choosing the nodes of the reduced finite element model. Additionally, the master node of the simplified model in the finite element method will produce the markers in the flexible structure [64][72]. From the Ansys APDL solution output, substructure files (sub and cdb) were created to represent the flexible underframe. These files are then used to generate an intermediate FBI (Flexible Body Interface) file for SIMPACK. Finally, the FBI file was imported into the multibody dynamic mode.

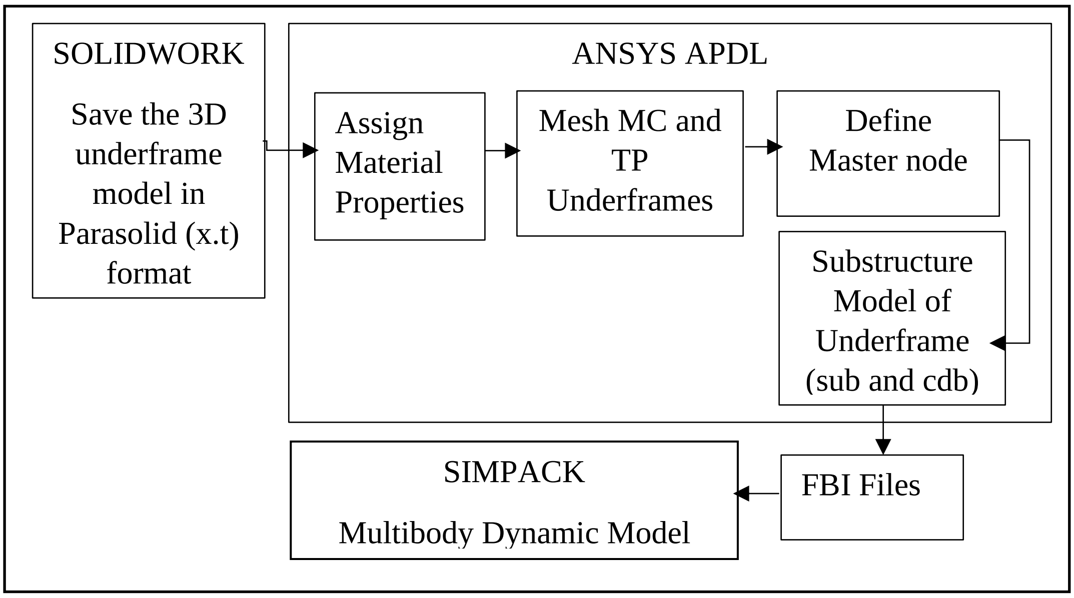

Figure 3.8 Integration of underframe 3D model into MBD model

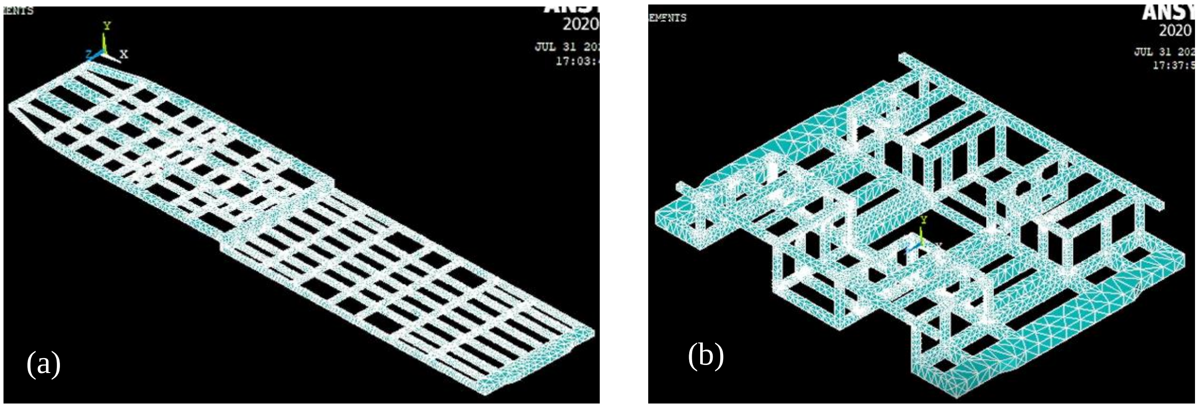

Figure 3.9 Mushing of (a) MC, and (b) TP underframe in ANSYS APDEL

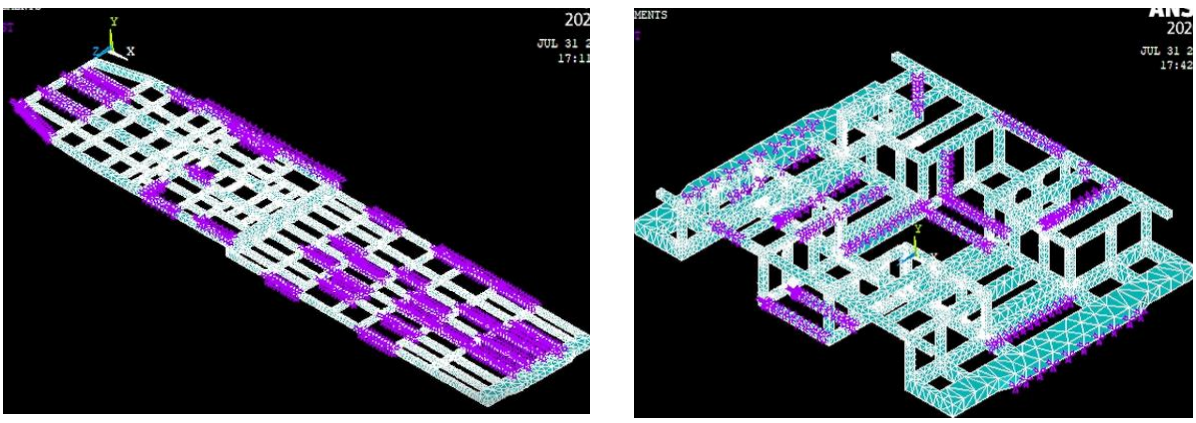

Figure 3.10 Defining Master nodes in ANSYS APDE

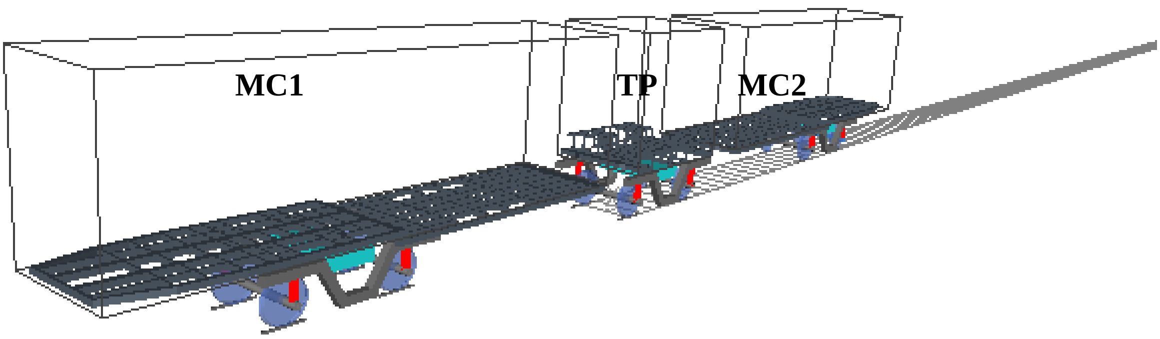

Figure 3.11 Front view of vehicle in MBDS

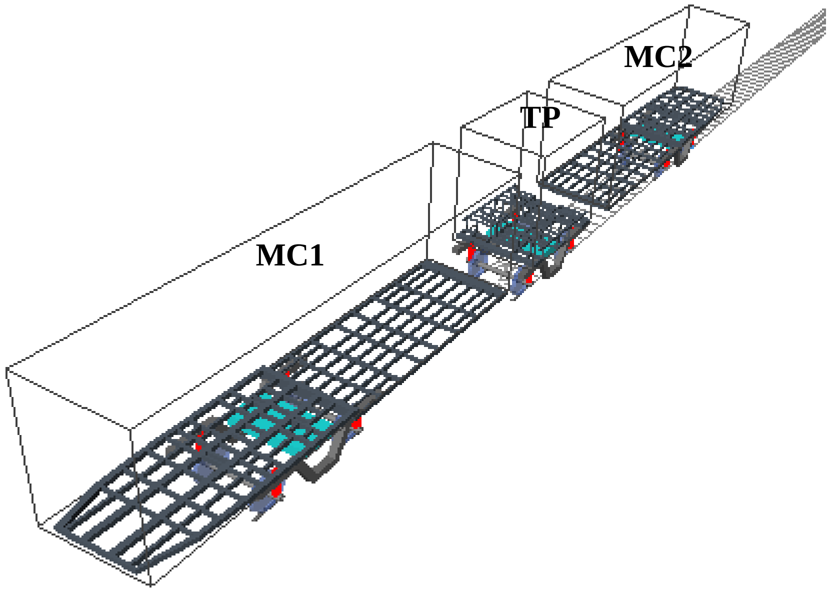

Figure 3.12 Isometric view of vehicle in MBDS

3.7 Simulation Parameter

The dynamic behaviour of the underframe structure when the vehicle is running on the irregular track was simulated by a detailed multibody dynamic model in SIMPACK. The simulation was performed on a 1000m straight track, where track irregularity data was incorporated into it. Simulations considered three vehicle speeds, 36 km/h, 50 km/h, and 70 km/h to examine the effect of speed on the chassis response. Each simulation has been performed for 30 seconds, with a 1000 Hz sampling frequency, to accurately capture the dynamic effects. From each simulation, acceleration-time history data consisting of 30003 data points were extracted at the selected locations of the underframe from the SIMPACK postprocessor. These acceleration-time histories were converted into force-time histories using Newton's second law for fatigue analysis of the underframe, as shown in Figures 3.13 and 3.14.

To validate the multibody dynamic simulation model, the dynamic responses of the underframe were compared against the limits specified in UIC 518. Each simulation procedure has been run for a simulation time of 30 seconds to finish the whole 1000m path on a HP Windows 10, 4GB Ram, 2.6 GHz processor laptop computer. The next chapter contains a detailed discussion of the simulation's results.

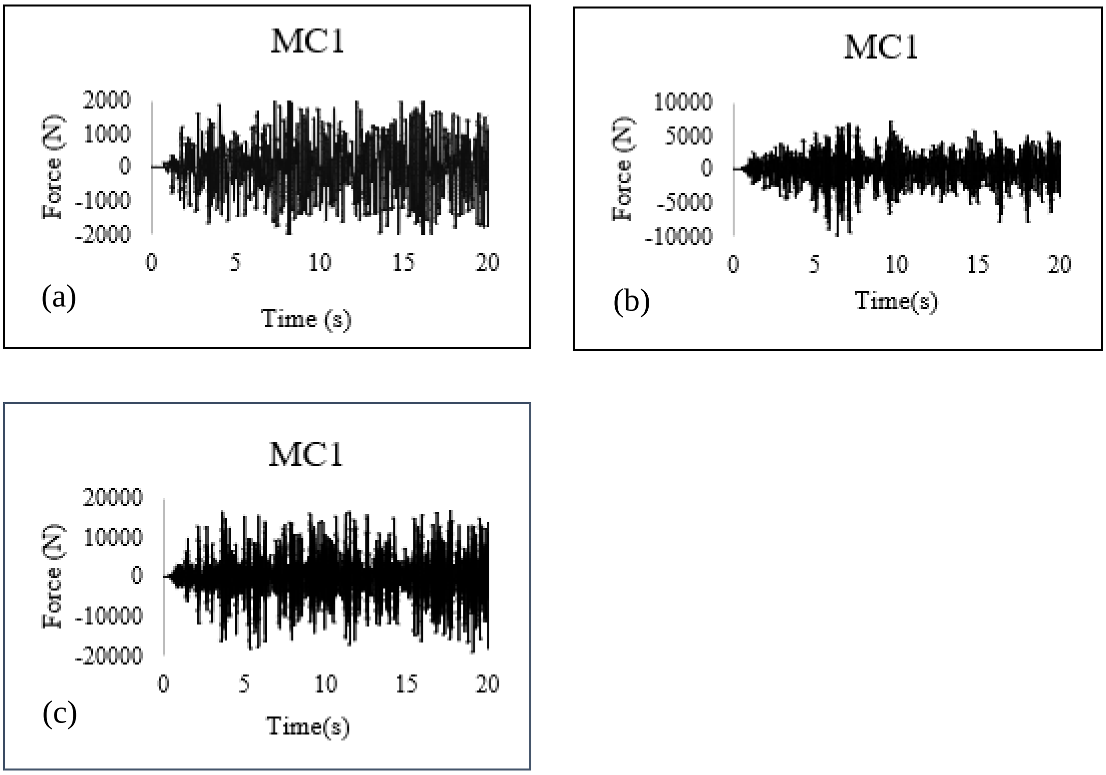

Figure 3.13 Vertical force of motor car (a) at 36km/h, (b) at 50 km/h, and (c) at 70km/h

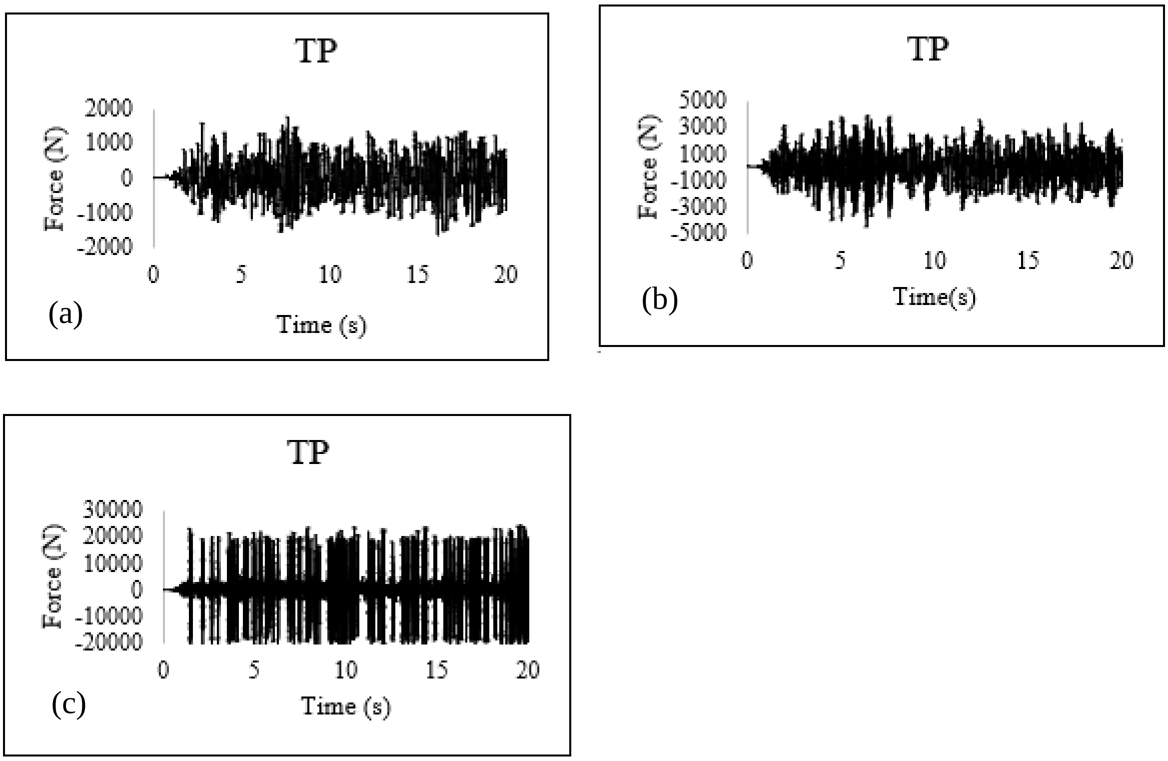

Figure 3.14 Vertical force of trailer car (a) at 36km/h, (b) at 50 km/h, and (c) at 70km/h

3.9 Finite Element Analysis

The foundation of car body fatigue analysis is the determination of the dynamic response of the car body structure. This dynamic response is commonly expressed in the form of a stress or strain time history. One of the standard approaches used to obtain the dynamic stress for fatigue life calculation is quasi-static stress analysis [68]. In this method external load history acting on the structure can be substituted by a static unit load at the same place and in the same direction as the load history. The quasi-static stress analysis is then executed for each unit load. Dynamic stresses for each distinct load history can be determined by multiplying the load history by the static stress influence coefficients (SICs) from the respective unit load [68], [73] The stress influence coefficient (SIC) is the stress generated by the unit load applied to the car body at the same location and in the same direction as the applied load histories. The mathematical representation of this approach, applied to a particular finite element configuration under plane stress conditions, is expressed as follows [68]:

$$\begin{bmatrix} \sigma_{xi}(t) \\ \sigma_{yi}(t) \\ \tau_{xyi}(t) \end{bmatrix} = \begin{bmatrix} \sigma_{x1}(t) & \sigma_{x2}(t) & \dots & \sigma_{xn}(t) \\ \sigma_{y1}(t) & \sigma_{y2}(t) & \dots & \sigma_{yn}(t) \\ \tau_{xy1}(t) & \tau_{xy2}(t) & \dots & \tau_{xyn}(t) \end{bmatrix} \begin{bmatrix} F_1(t) \\ F_2(t) \\ \vdots \\ F_n(t) \end{bmatrix} \tag{3.1}$$

where F_i (t) is the number of load histories, n is the number of load histories, and σ_{xi}, σ_{yi} , τ_{xyi} are the stress effect coefficients.

The underframe's fatigue life was estimated by combining multibody dynamic simulations with FEM analysis. Applying Newton's second law (F = ma), force time histories were calculated using the dynamic responses derived from the simulations.

To estimate fatigue life, a quasi-static stress analysis was performed. Unit loads (1N) were applied at selected areas of the underframe to obtain stress distributions. These stress results were exported to Ansys n-Code Design Life for fatigue analysis. Then, dynamic loads at the same locations and directions as the unit loads were applied to the model to predict fatigue life.

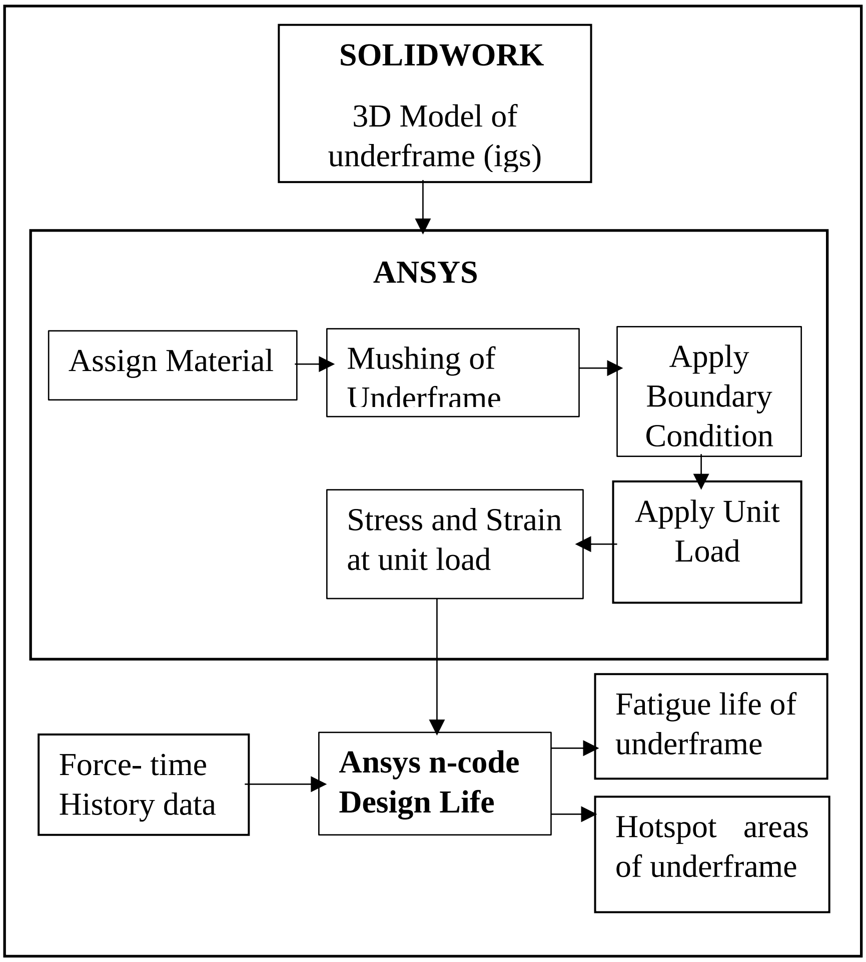

Figure 3.15 Fatigue life methodology flow chart

In the FEM analysis, the mesh size of 20 mm was used to get the necessary results. The MC underframe was meshed with 1073407 nodes and 674395 elements, while the TP underframe consisted of 516255 nodes and 326069 elements. The mesh independence analysis was done on both MC and TP underframes, and both underframe models was converged in under allowable change of 2% for von-miss stress.

The boundary conditions were applied as fixed support at the bolster area of both frames, as shown in Figure 3.18, and the unit loads were then applied to the critical region of the frames. And finally, the resulting stresses at unit load (1N) were solved for fatigue life analysis as illustrated in Figure 3.20.

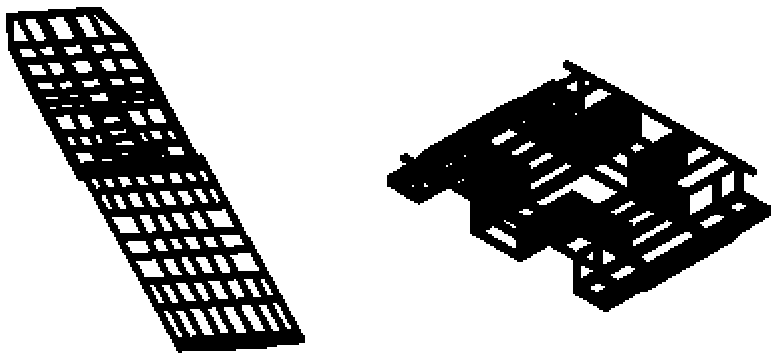

(a) (b)

Figure 3.16 Mushing of (a) MC1 and (b) TP underframe

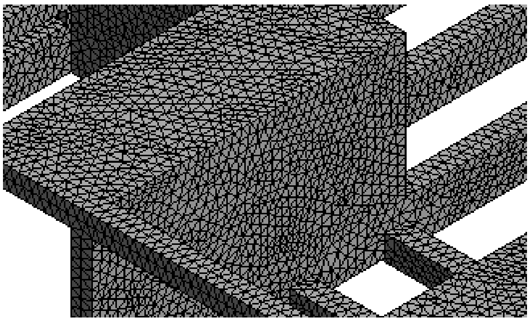

Figure 3.17 Enlarged view of underframe mesh

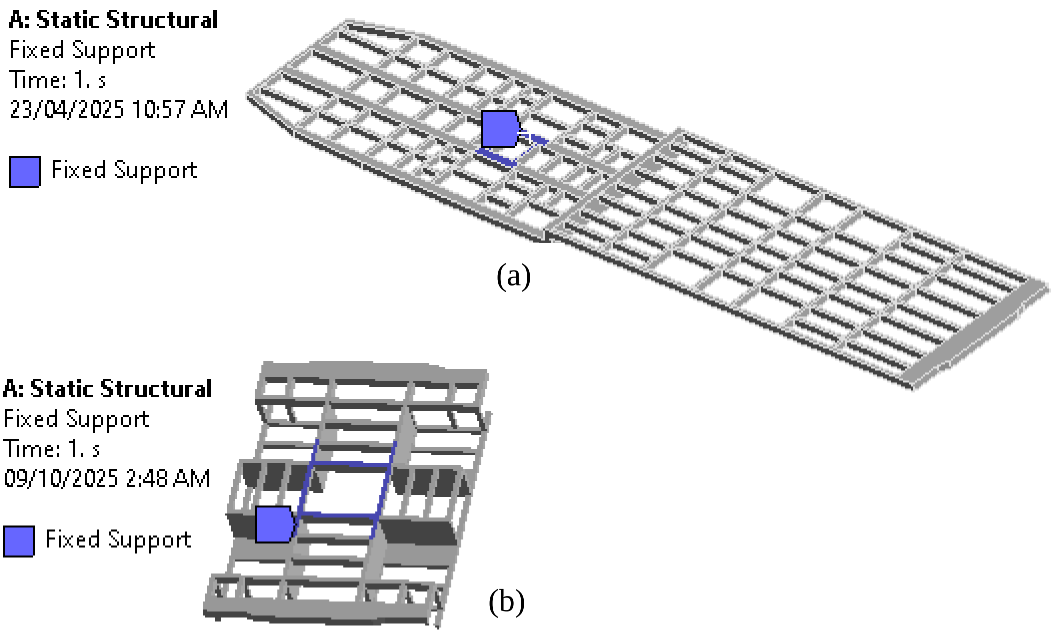

(a)

(b)

Figure 3.18 Boundary condition of (a) MC1 and (b) TP underframe

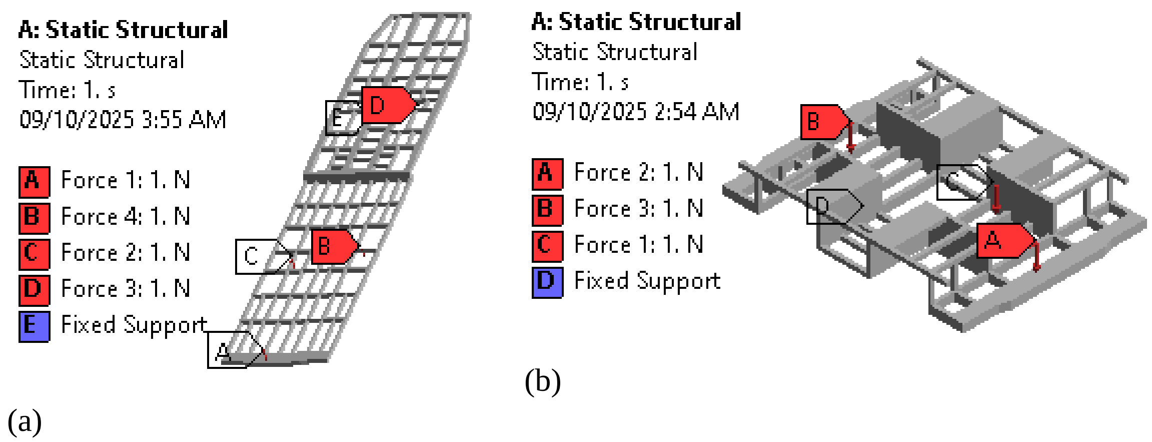

Figure 3.19 Unit load application (a) MC1 and (b) TP underframe

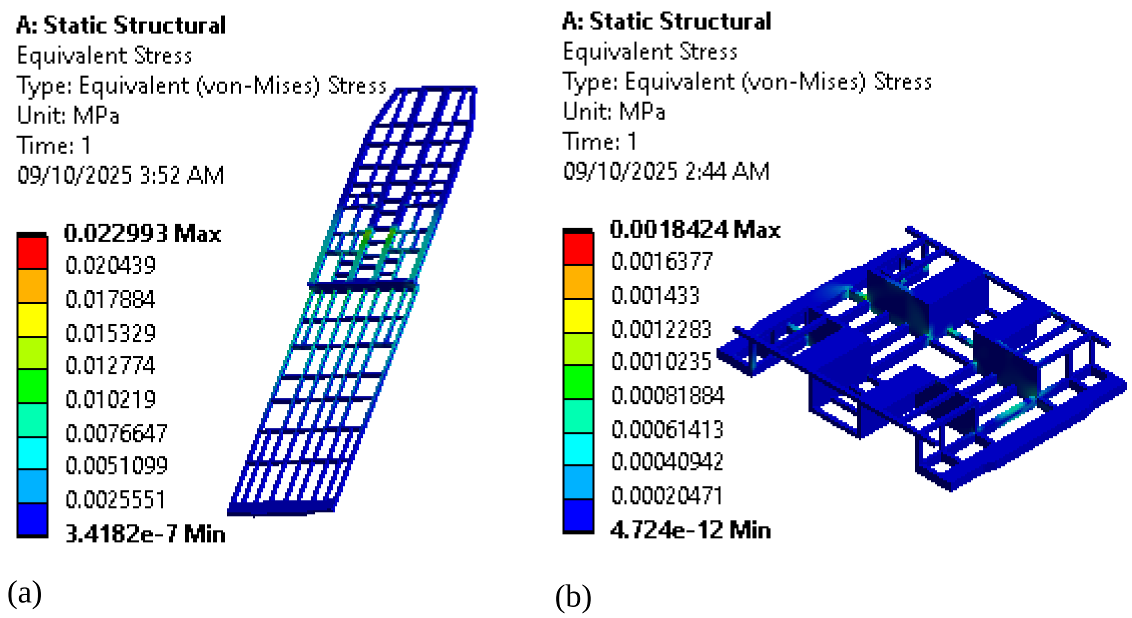

Figure 3.20 Stress Distribution of (a) MC1 and (b)TP underframe at unit load

CHAPTER 4- RESULTS AND DISCUSSION

4.1 Result

This chapter presents the simulation and analysis results conducted to examine the effect of track irregularities on the light rail vehicle underframe car body structure. The dynamic response of the underframe due to track imperfections for three speed cases is presented in the first section. These findings offer important insights about the influence of track deviations on the structural behavior of the underframe and form the foundation for the following fatigue life predictions. The second section describes the simulated underframe fatigue life prediction from ANSYS n-Code design life by using the simulated dynamic load history. The third section presents the key stress concentration nodes in the underframe. Finally, the chapter compares the simulated fatigue life of the underframe to the calculated fatigue life to validate the results. The discussion presents these results with appropriate explanation to address the objective of the study.

4.2 Effect of Track Irregularities on Underframe Dynamic Behavior

This section presents the dynamic behaviour of the underframe under track irregularity excitation at vehicle speed of 30 km/h, 50 km/h, and 70 km/h. The responses, specifically the vertical and lateral accelerations of the front motor car (MC1), trailing car (TP), and rear motor car (MC2) underframe, are examined to understand their behaviour due to the track irregularities. The simulation results are presented as vertical and lateral acceleration time histories.

Case 1: Dynamic response of underframe at speed of 36 km/h

The dynamic response of the underframe due to the effect of track irregularities at a vehicle speed of 36km/h was analysed, as shown in Figures 4.1 and 4.2, which present the vertical and lateral acceleration responses for the three chassis sections. Vertical accelerations are consistently higher than lateral accelerations across all underframe structures, with maximum values of 0.307 m/s^2, 0.182 m/s^2, and 0.324 m/s^2 for MC1, TP, and MC2, respectively, compared to corresponding maximum lateral accelerations are 0.189 m/s^2, 0.143 m/s^2, and 0.193 m/s^2.

Motor car underframes experience greater accelerations in both vertical and lateral directions compared to the trailer car. This behaviour arises from the structural and mass characteristics of motor cars, which make them more susceptible to dynamic excitation, and their positions at the front and rear ends of the vehicle. Motor cars experience the initial input disturbances directly since they are the first and last to encounter track abnormalities. On the other hand, the centrally located trailer car experiences a partially damped and filtered response since the motor car moderates the irregularities. As a result, motor car underframes are more affected by track imperfections than trailer cars.

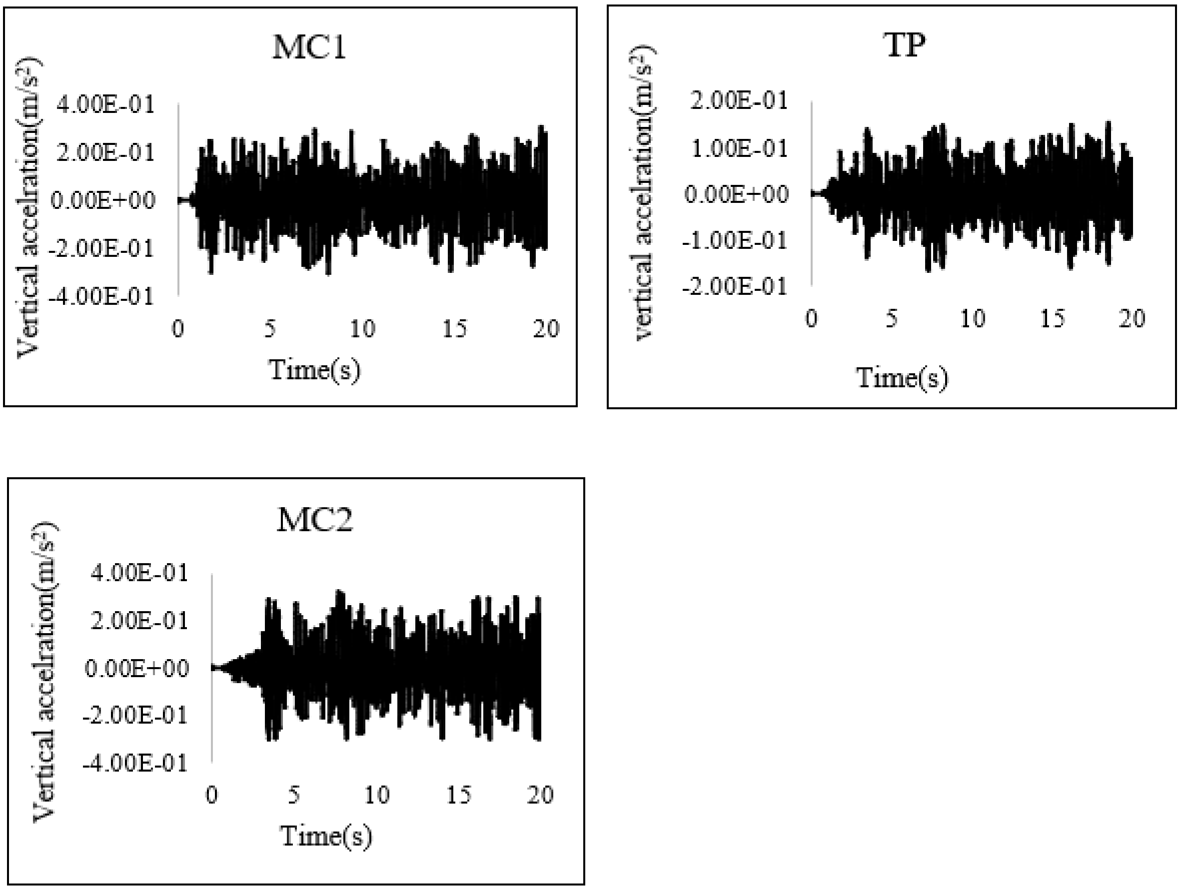

Figure 4.1 Vertical acceleration of MC1, TP and MC2 underframe at 36km/h

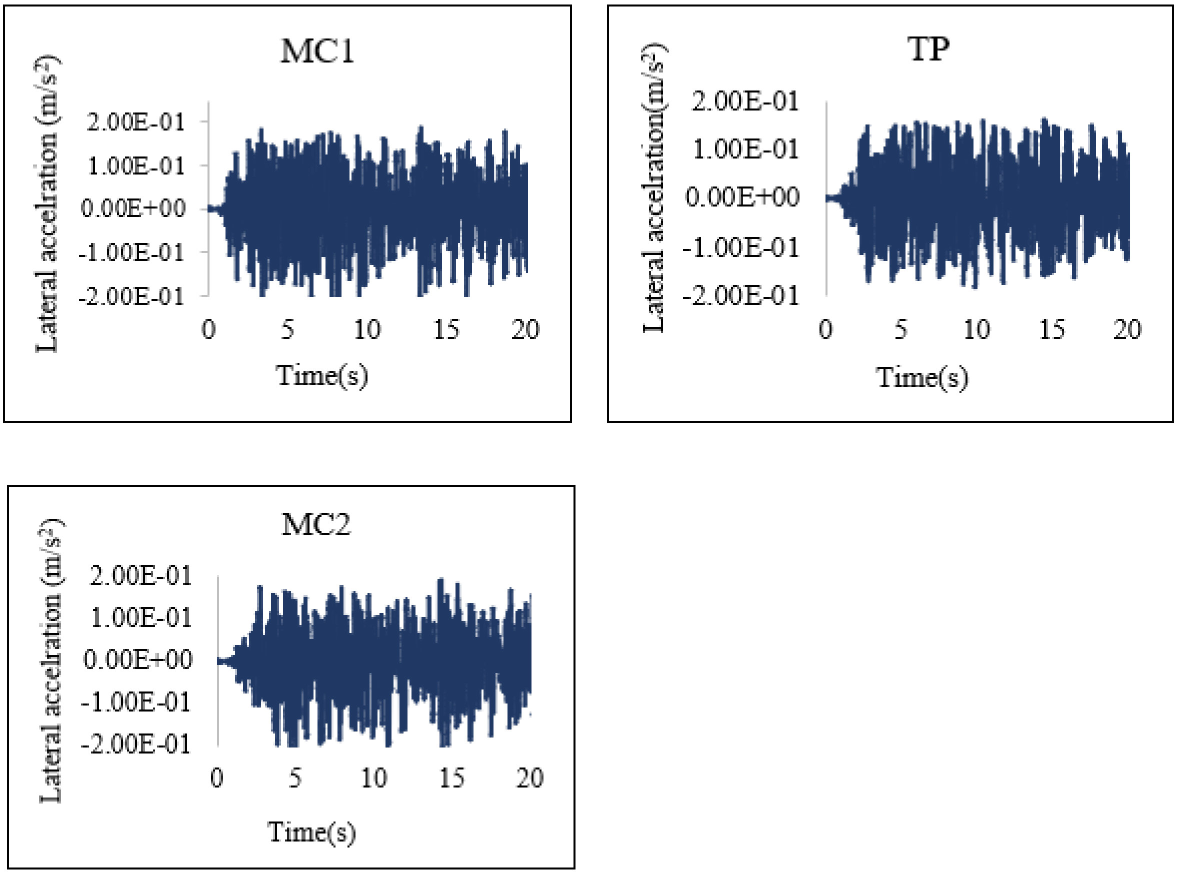

Figure 4.2 Lateral acceleration of MC1, TP and MC2 underframe at 36km/h

Case 2: Dynamic response of underframe at speed of 50 km/h

Figures 4.3 and 4.4 present the underframe dynamic response to track irregularities at a vehicle speed of 50 km/h. The maximum vertical accelerations are 0.989 m/s^2, 0.383 m/s^2, and 0.975 m/s^2 for MC1, TP, and MC2, respectively, whereas the corresponding maximum lateral accelerations are 0.398 m/s^2, 0.309 m/s^2, and 0.343 m/s^2. Compared with the results at 36 km/h, these values show a clear increase in dynamic excitation with speed; i.e., higher operating speeds increase vertical as well as lateral accelerations of the underframe. In both motor car and trailer car underframes, vertical accelerations are consistently greater than lateral ones, indicating that track irregularities have a greater impact in the vertical direction. Furthermore, the motor car underframe shows greater sensitivity to dynamic excitation than the trailer car, consistent with the response observed at 36 km/h. This confirms that MC underframes are more susceptible to vibration and dynamic loading caused by track deviations.

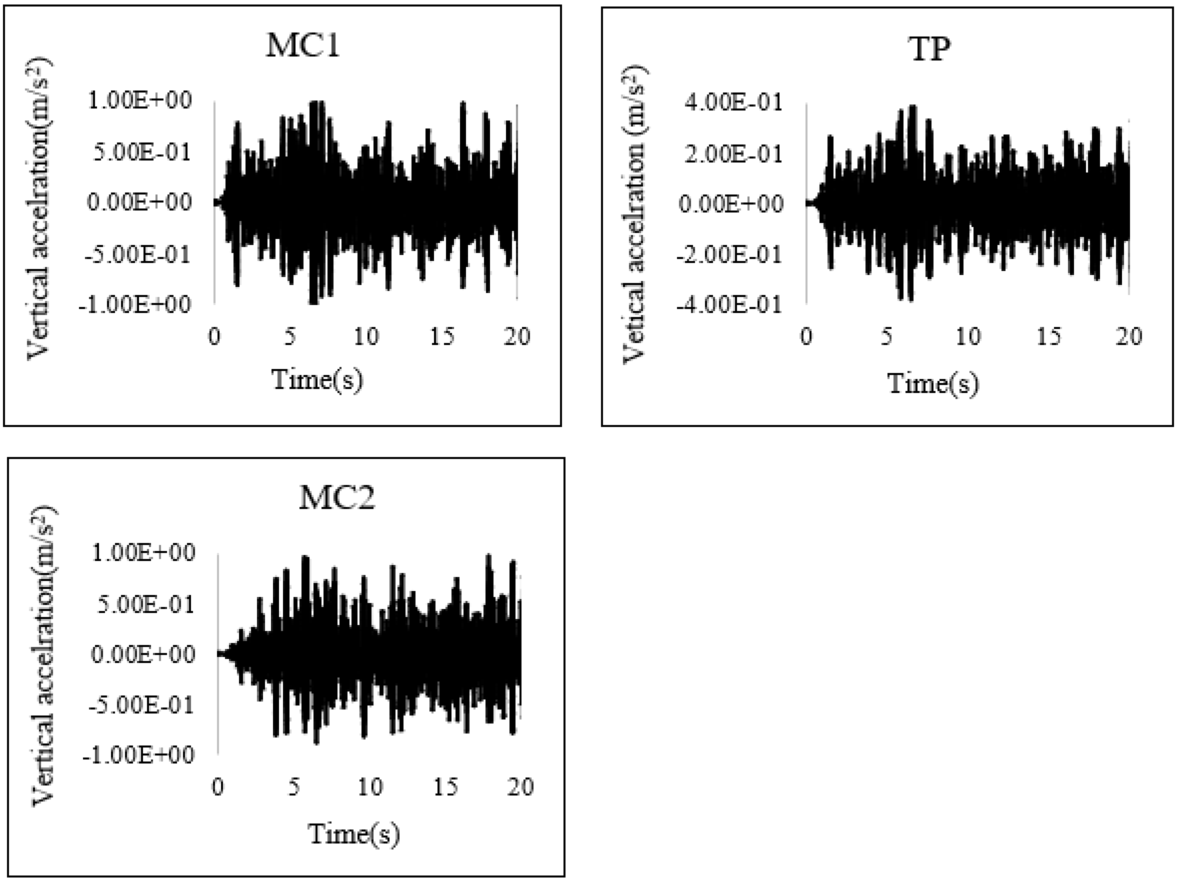

Figure 4.3 Vertical acceleration of MC1, TP and MC2 underframe at 50km/h

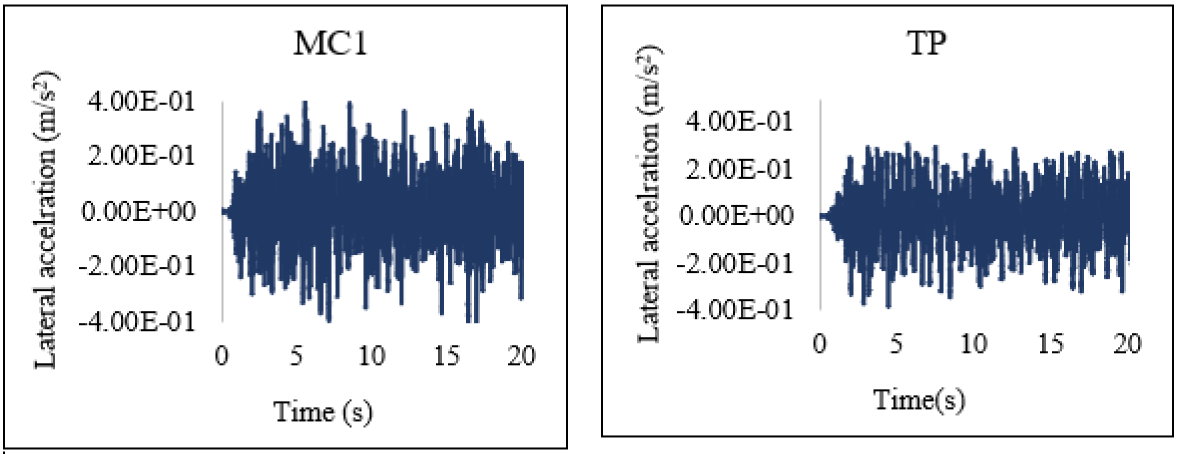

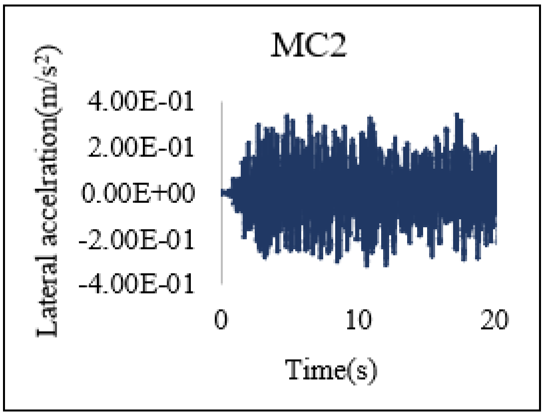

Figure 4.4 Lateral acceleration of MC1, TP and MC2 underframe at 50km/h

Case 3: Dynamic response of underframe at speed of 70 km/hr

When the vehicle speed is increased to 70 km/h, the underframe dynamic response to track irregularities becomes more significant. The resulting lateral and vertical accelerations for the three chassis structures are displayed in Figures 4.5 and 4.6.

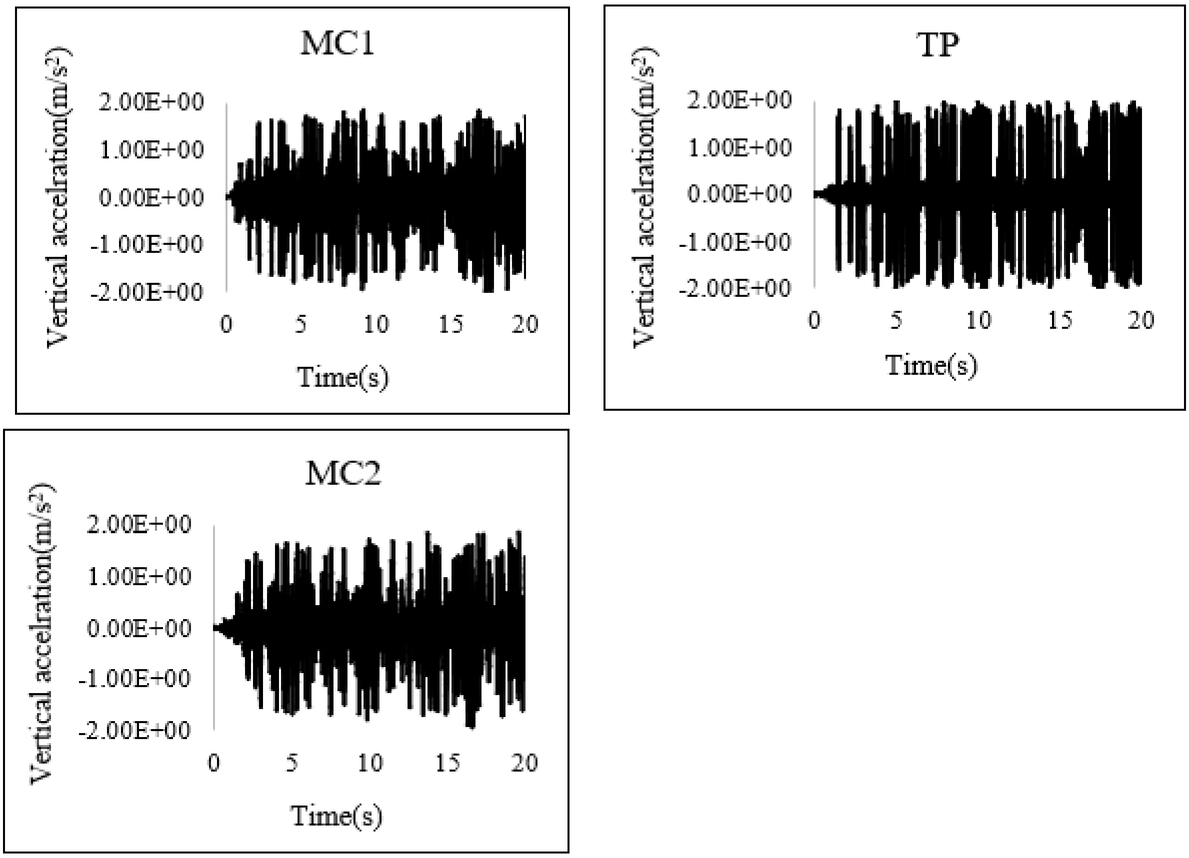

Figure 4.5 Vertical acceleration of MC1 TP and MC2 underframe at 70 km/h

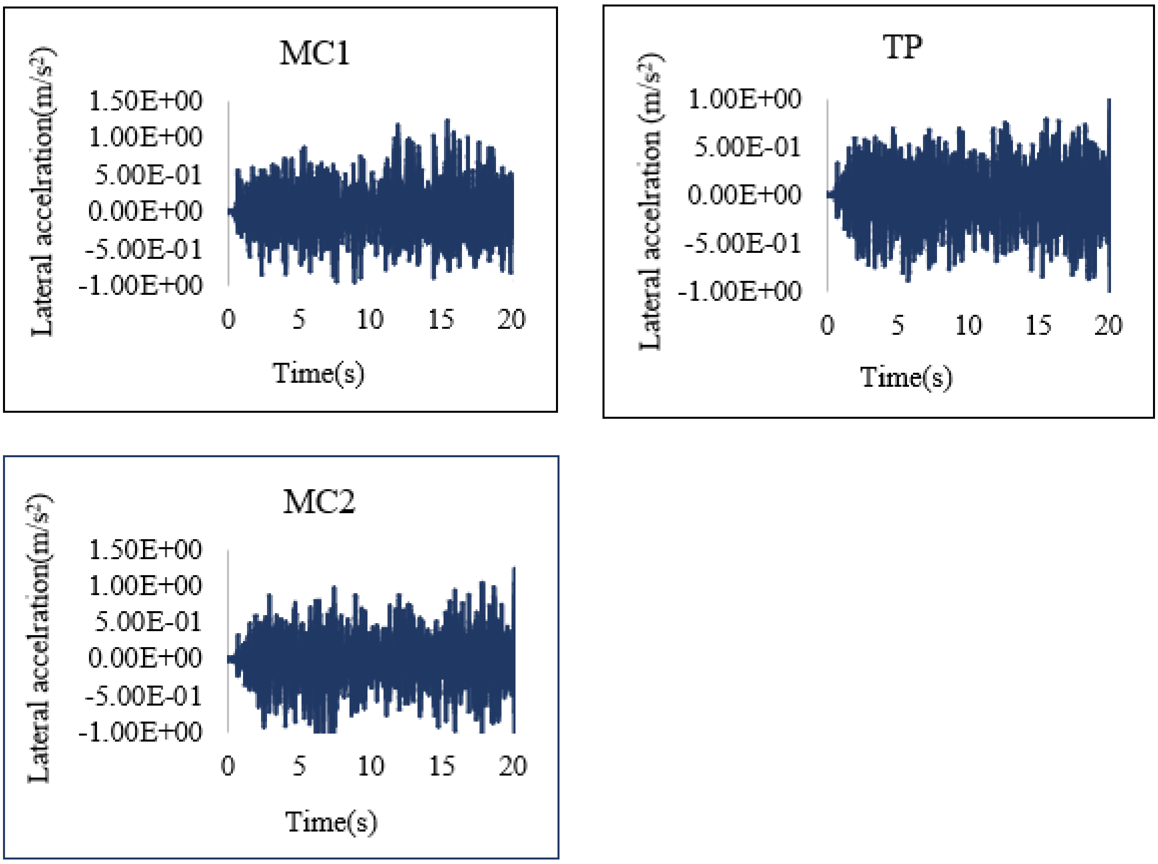

Figure 4.6 Lateral acceleration of MC1, TP and MC2 underframe at 70km/h

The maximum vertical accelerations are 1.91 m/s², 1.80 m/s², and 1.87 m/s² for MC1, TP, and MC2, respectively, whereas the corresponding maximum lateral accelerations are 1.23 m/s², 0.781 m/s², and 1.04 m/s². These results confirm that vertical accelerations are continuously higher than lateral ones across all underframe structures, as in the previous cases. Additionally, the motor car underframes are more affected by track irregularities compared to the trailer car, which is consistent with the previous speed cases results.

From the three speed cases examined above, there is an observed common trend: as operating speed increases, the vertical and lateral accelerations increase as well, which is consistent with the pervious researches [74][75][76]. This implies that the effect of track irregularities becomes more significant at higher vehicle speeds.

This occurs mainly due to the excitation frequency induced by the track irregularities. This excitation frequency (f) is directly proportional to the vehicle operating speed (v) and inversely proportional to the track irregularity wavelength (λ) [77]; which can be expressed as:

$$f = \frac{v}{\lambda}. \quad 4.1$$

As the operating speed of the vehicle increases, the excitation frequency generated by the track irregularities also increases. When this excitation frequency approaches natural frequency of the vehicle (1 Hz), the dynamic responses of the vehicle increase significantly[77].

According to the Chinese standard for operational comfort, the vertical acceleration of the vehicle body should not exceed 0.13 g (≈1.275 m/s²) [78]. The underframe response remains within this limit when the vehicle operates at 36 km/h and 50 km/h; however, at 70 km/h, the underframe vertical acceleration exceeds this limit (1.91 m/s², 1.80 m/s², and 1.87 m/s² for MC1, TP, and MC2, respectively). Although this study does not focus on ride comfort, exceeding this limit proves that the dynamic excitation increases at higher speeds. Generally, the results show that track irregularities at higher speeds induce stronger excitation forces, which lead to greater structural vibrations.

Table 4.1 Summery of maximum accelerations

Speed (km/h)	Accelerations	Underframe configurations		
		MC1 (m/s^2)	TP (m/s^2)	MC2 (m/s^2)
36 km/h	Vertical	0.307	0.182	0.324
	Lateral	0.189	0.143	0.193
50 km/h	Vertical	0.989	0.383	0.975
	Lateral	0.398	0.309	0.343
70 km/h	Vertical	1.91	1.80	1.87
	Lateral	1.23	0.781	1.04

In order to verify the accuracy of the multibody dynamic simulation model, the car body acceleration responses for the vehicle were verified against limits specified in UIC 518. Under UIC 518, it is required that the vertical and lateral car body accelerations should not exceed 2.5 m/s² for safe running [79]. As shown in Table 4.1, the maximum accelerations of the underframe car body in the simulation were all under the specified value, confirming that the model accurately captures the dynamic response of the vehicle under irregular track conditions.

4.3 Fatigue Life of Underframe

The fatigue life of the underframe was estimated using the FEM software Ansys n-Code Design Life. The analysis was performed at vehicle speeds of 36 km/h, 50 km/h, and 70 km/h, and the corresponding results are given in Figures 4.7, 4.8, and 4.9. For motor car underframe, the predicted fatigue life is $2.59e^9$, $2.45e^7$, and $1.36e^5$ cycles at 36km/h, 50km/h, and 70 km/h, respectively. For the trailer car, the corresponding fatigue life is $3.10e^{10}$, $1.12e^8$, and $7.76e^5$ cycles at the same operating speeds. These results show that underframe fatigue life decreases significantly with increased vehicle speed. The highest fatigue life for both the MC and TP underframes occurs at 36 km/h, while the lowest is at 70 km/h.

This is because with higher speeds, there is increased dynamic loading that leads to greater fatigue damage within the structure.

Operating speed has an important influence in the fatigue durability of rail vehicles car body, higher speeds significantly reduce the car bodies service life. As shown in Figure 4.7, at 36 km/h, the MC underframe achieved a fatigue life of $2.59e^9$ cycles, while the TP reached $3.10e^{10}$ cycles, indicating a longer life for the TP underframe under the same operating conditions. When the speed increased to 50 km/h, fatigue life of both underframes decreased significantly, with MC decreased to $2.45e^7$ cycles and TP to$1.12e^8$ cycles. The most severe reduction occurred at 70 km/h, where the MC underframe predicted life declined to $1.36e^5$ cycles and the TP to $7.76e^5$ cycles. At all speeds, the TP underframe had a higher fatigue life than MC.

When the vehicle operating speed increases from the lowest vehicle speed (30 km/h) to the maximum vehicle speed (70 km/h) the fatigue life of the underframe decreased significantly, as shown in Figures 4.7, 4.8, and 4.9. This trend is consistent with the dynamic response of the underframe due to track irregularity excitations. As the vehicle speed increases, the excitation frequency from the irregular track geometry approaches the natural frequency of the underframe. This leads to higher dynamic stresses in the underframe. The higher dynamic stresses cause fatigue damage accumulation, and gradually decrease the fatigue life of the underframe.

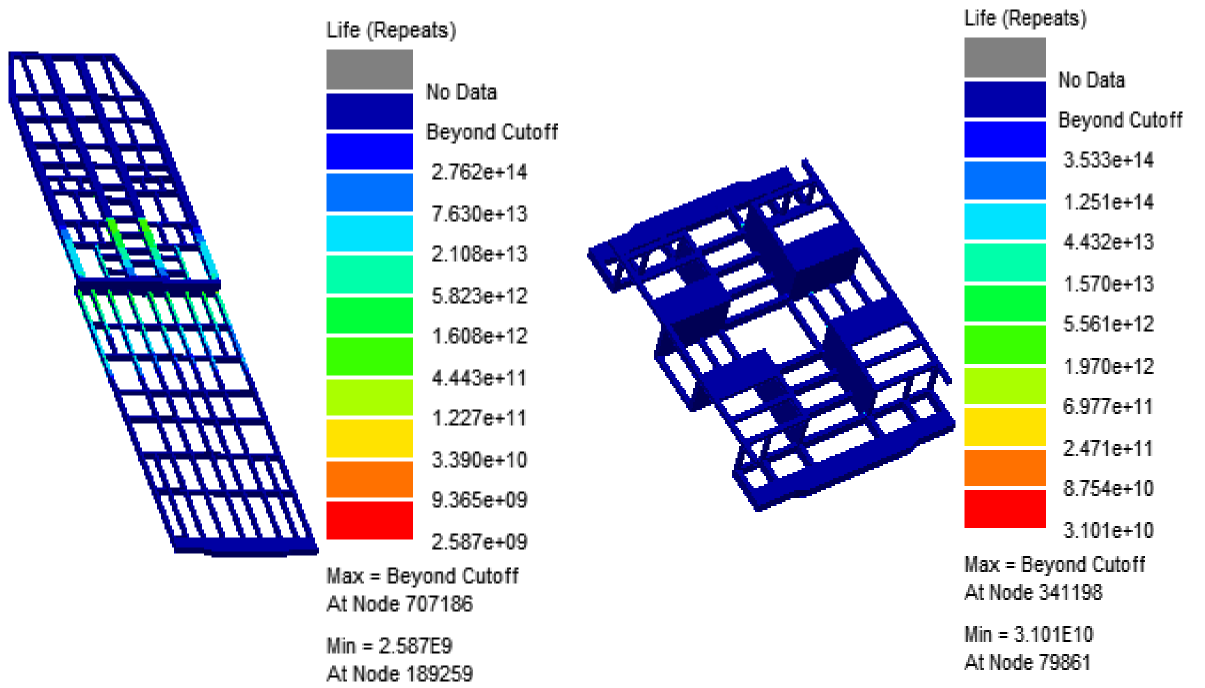

Figure 4.7 Fatigue life of MC and TP underframes at 36 km/h

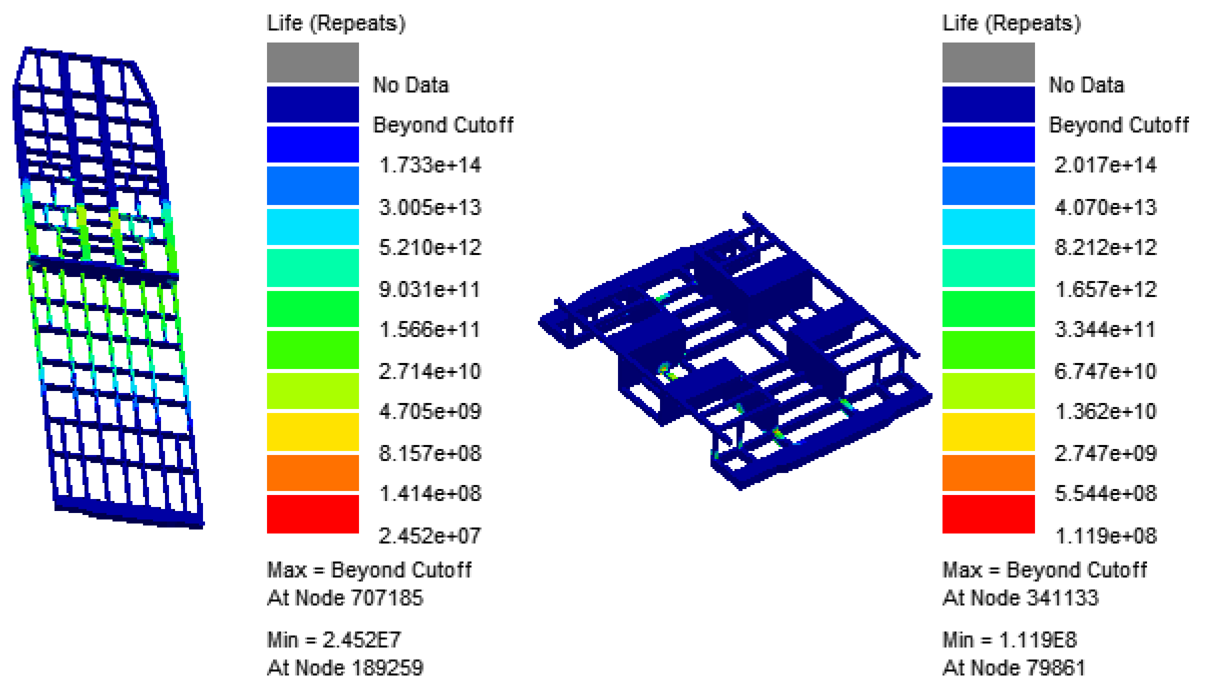

Figure 4.8 Fatigue Life of MC and TP underframes at 50 km/h

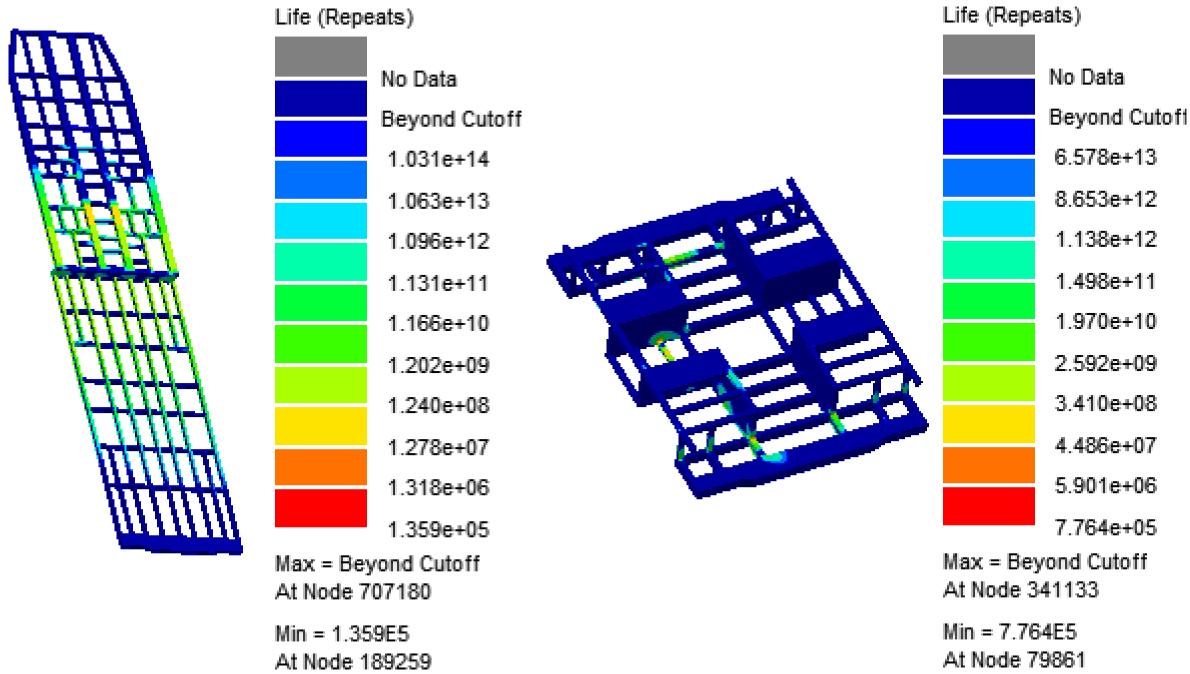

Figure 4.9 Fatigue Life of MC and TP underframes at 70 km/h

The fatigue life analysis results clearly show that the effect of track irregularities increases with vehicle running speed and correspondingly reduces underframe fatigue life. The design life of underframe is greater than 1×10^7cycles, equivalent to approximately 30 years of service [80]. Both MC and TP underframes satisfy this requirement at 36 km/h and 50 km/h running speeds. However, at 70 km/h, the estimated fatigue life falls below this limit, and therefore, the effect of track irregularities is severe at this speed.

4.4 Stress Concentration Nodes in Underframe

Stress concentration nodes (hotspots) are nodes that have significantly higher stress than the surrounding nodes, which can lead to fatigue failure. These hotspots are significant to engineers to determine where design improvements should be implemented for increased durability. The MC and TP underframe hotspots are identified by using Ansys n-Code Design Life based on fatigue life analysis. The MC underframe hotspot nodes are presented in Figure 4.10, where the most critical nodes are highlighted and the corresponding damage values for all operating speeds are summarized in Table 4.2.

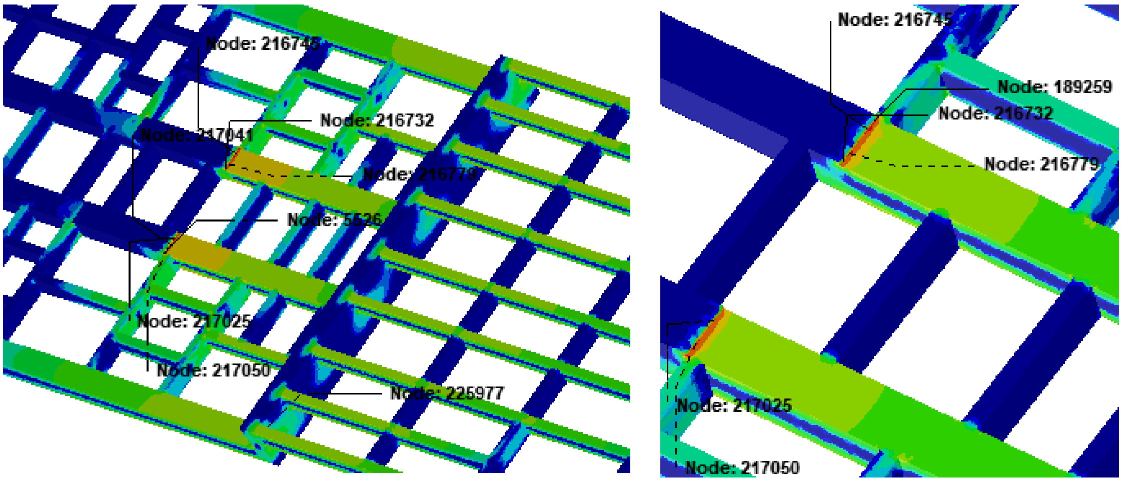

Figure 4.10 Hotspot nodes in MC underframe

The most critical hotspot nodes are consistently found in the **high-floor area**, particularly at bolster area, as shown in the Figure 4.11. This indicate that the high floor area governs the fatigue performance of the MC underframe, whereas the low-floor area remains less affected.

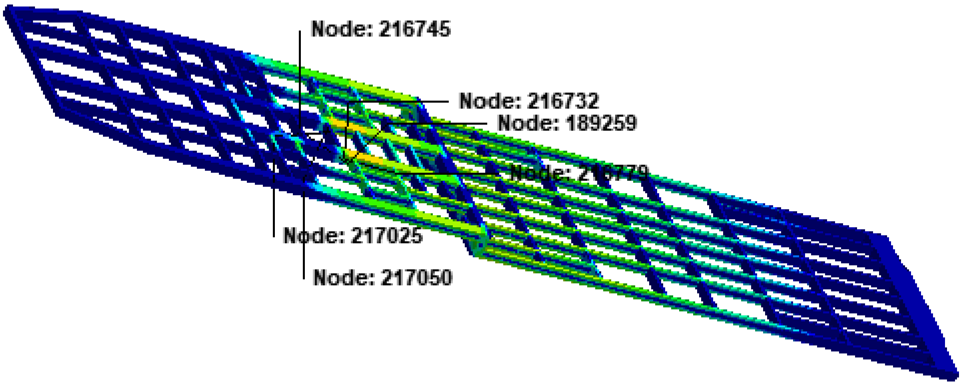

Figure 4.11 Hotspots on the MC underframe concentrated at the high-floor area.

At all operating speeds, fatigue damage is localized at a few key nodes, as shown in Table 4.2 At 36 km/h, the damage is minor and within the design threshold, but when the speed increases to 50 km/h and 70 km/h, these key nodes experience a sudden rise in damage, reaching 10^{-6} at the highest speed. **Node 189259** is identified as the most critical hotspot under all the operating conditions, and therefore the most probable site for fatigue failure. The fatigue life of this node at 70 km/h is $1.36e^{5}$ cycles, as shown in Figure 4.9, which is below the acceptable threshold. This critical node is followed by **nodes 216745 and 217050**, which also exhibit relatively higher fatigue damage compared to the other nodes.

Table 4.2 Fatigue damage of hotspot nodes on MC1 underframe at various vehicle speeds.

No	Node	Damage		
		At 36 km/h	At 50 km/h	At 70km/h
1	189259	3.865E-10	4.079E-8	7.357E-6
2	216745	2.752E-10	2.904E-8	5.237E-6
3	217050	2.378E-10	2.509E-8	4.525E-6
4	216779	2.106E-10	2.222E-8	4.008E-6
5	216732	1.432E-10	1.511E-8	2.725E-6
6	217025	1.406E-10	1.484E-8	2.677E-6
7	5526	1.179E-10	1.244E-8	2.244E-6
8	216755	9.412E-11	9.934E-9	1.792E-6
9	217041	7.998E-11	8.441E-9	1.522E-6
10	225977	2.157E-11	2.278E-9	4.109E-7

Similarly, TP underframe hotspot nodes are illustrated in Figure 4.12, and the corresponding damage values are listed in Table 4.3 for the three vehicle speeds. At 36 km/h, the damage remains negligible and within safe design limits. At 50 km/h and 70 km/h, however, these nodes show a significant increase in damage at the maximum speed. Among them, **node 79861** is the most critical node with a fatigue life of $7.76e^{5}$ cycles at 70 km/h, indicating a potential risk of fatigue failure. **Node 79861** is followed by **nodes 104839, 113206, and 127107**, which also exhibit relatively higher damage compared to the rest.

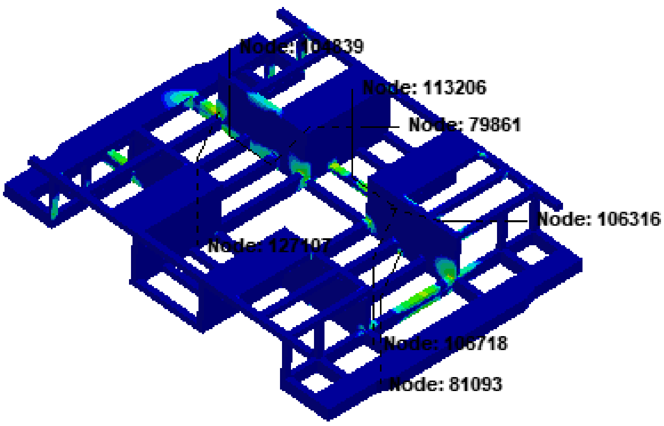

Figure 4.12 Hotspot nodes in TP underframe

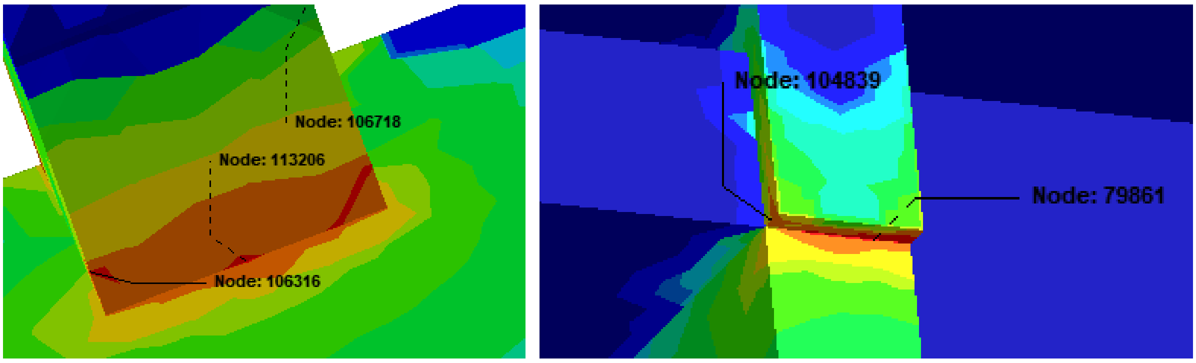

Figure 4.13 Enlarged picture of hotspot nodes in TP underframe

Table 4.3 Fatigue damage of hotspot nodes on TP underframe at various vehicle speeds

		Damage		
No	**Node**	At 36 km/h	At 50 km/h	At 70 km/h
1	79861	3.225E-11	8.939E-9	1.288E-6
2	104839	7.158E-12	1.992E-9	2.871E-7
3	113206	6.629E-12	1.845E-9	2.659E-7
4	127107	6.567E-12	1.828E-9	2.634E-7
5	106728	6.433E-12	1.791E-9	2.581E-7
6	106316	6.026E-12	1.678E-9	2.418E-7
7	81093	1.56E-12	4.422E-10	6.373E-8
8	3983	1.191E-12	3.395E-10	4.893E-8
9	106718	9.903E-13	2.843E-10	4.098E-8
10	117563	2.956E-13	9.207E-11	1.328E-8

4.5 Validation of Fatigue Life Simulation

To validate the accuracy of the fatigue life simulation in ANSYS n-Code Design Life, the fatigue life is also calculated using Smith-Watson-Topper (SWT) modified form of Manson-Coffin approach. This method considers stresses as well as strains induced in the structure. The results from the simulation are validated with the results obtained from the SWT analytical calculation. The expression for the SWT fatigue life approach is presented in Equation (4.1) [81] .

$$\sigma_{\max}\frac{\Delta\varepsilon}{2} = \frac{(\sigma'_f)^2}{E}(2N_f)^{2b} + \sigma'_f\,\varepsilon'_f\,(2N_f)^{b+c} \qquad 4.2$$

The symbols εf, $\sigma f'$, c and b represent various fatigue properties; the fatigue coefficient of ductility, fatigue coefficient of strength, fatigue exponent of ductility and fatigue strength exponent, respectively. While σ_{max}, $\Delta\varepsilon/2$, N_f and E stand for maximum stress, strain amplitude, fatigue life cycles and modulus of elasticity, respectively [81] .

The underframe steel material fatigue properties were adopted from [27], with $\sigma f'$=930 MPa, $\varepsilon f'$=0.298, b=−0.106, c=−0.49, and the modulus of elasticity as E=204GPa [50]. Based on these parameters, the fatigue life was calculated using Python programming and compared with simulation results from ANSYS n-Code Design Life.

The maximum dynamic forces in the underframe were applied to the FEM model in ANSYS workbench, to get the maximum stress (σ_{max}) and strain amplitude ($\Delta\varepsilon/2$) on the underframe for each operating speed condition, which were then used in the calculation of the fatigue life. The strain amplitude was calculated using equation 4.2 [82]:

$$\Delta\varepsilon/2 = \frac{\varepsilon_{max} - \varepsilon_{min}}{2} \qquad 4.3$$

Figures 4.14, 4.15, and 4.16 (a–f) illustrate stress distribution, while, Figures 4.17, 4.18, and 4.19 (a–f) show strain distribution of both MC and TP underframe at operating speeds of 36 km/h, 50 km/h, and 70 km/h, respectively. The corresponding maximum stress and strain amplitudes are summarized in Table 4.4.

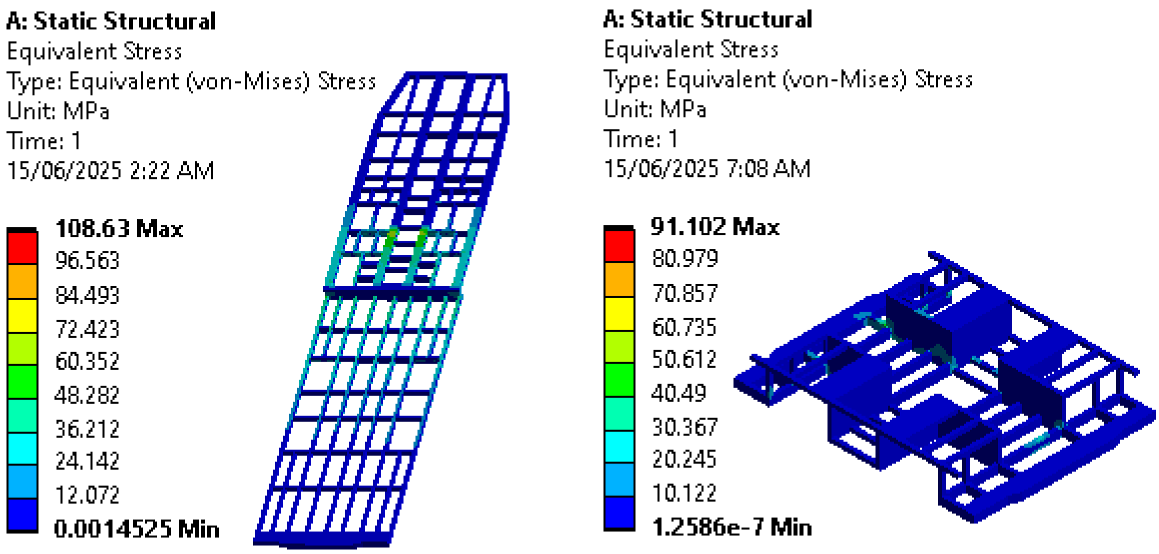

(a) (b)

Figure 4.14 Stress Distribution of (a) MC1, and (b) TP underframe at 36 km/h

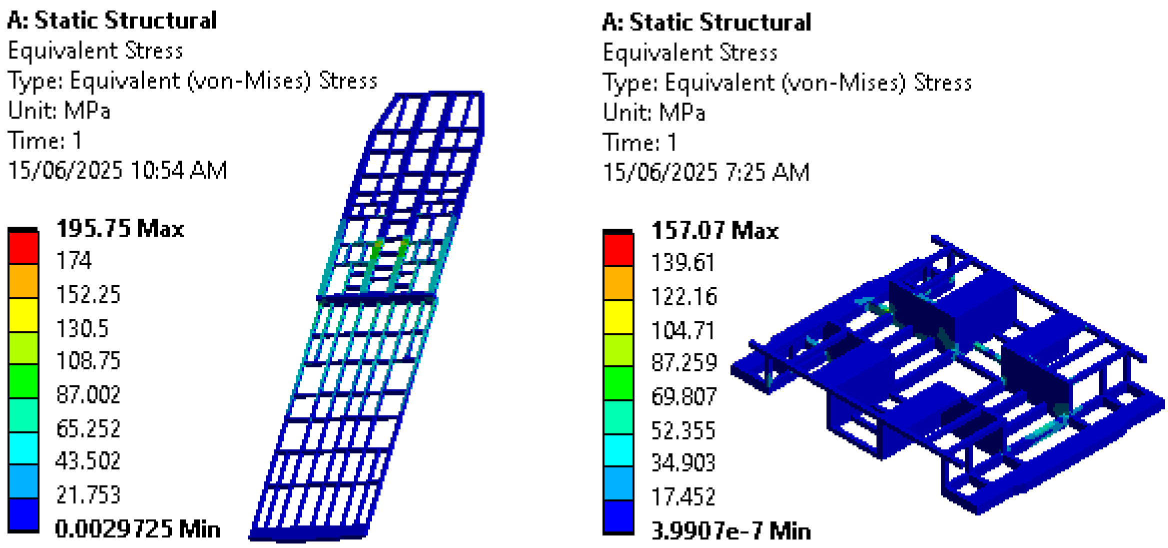

(c) (d)

Figure 4.15 Stress Distribution of (a) MC1, and (b) TP underframe at 50 km/h

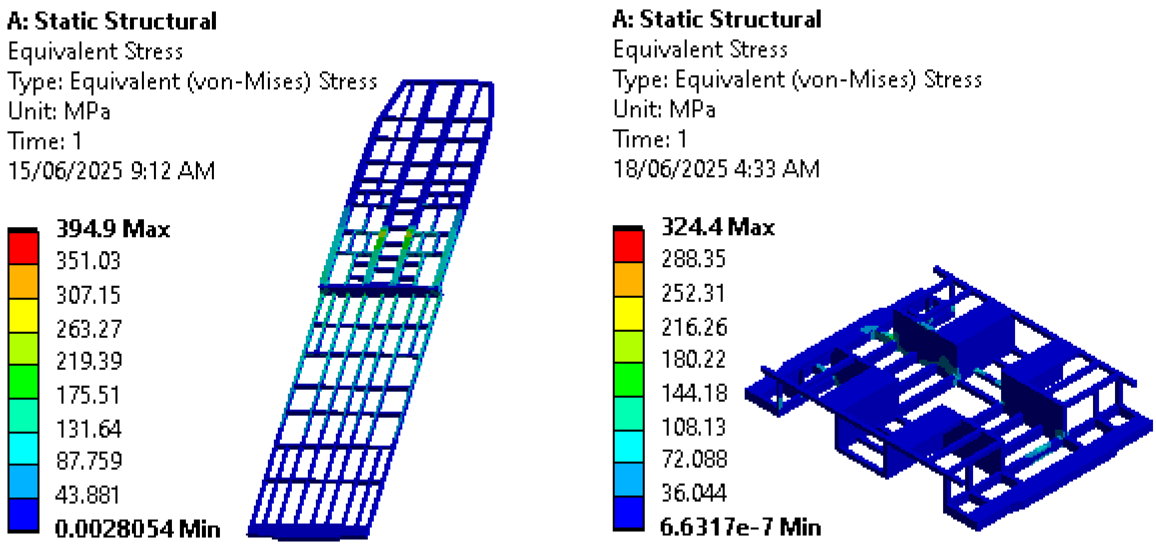

(e) (f)

Figure 4.16 Stress Distribution of (a) MC1, and (b) TP underframe at 70 km/h

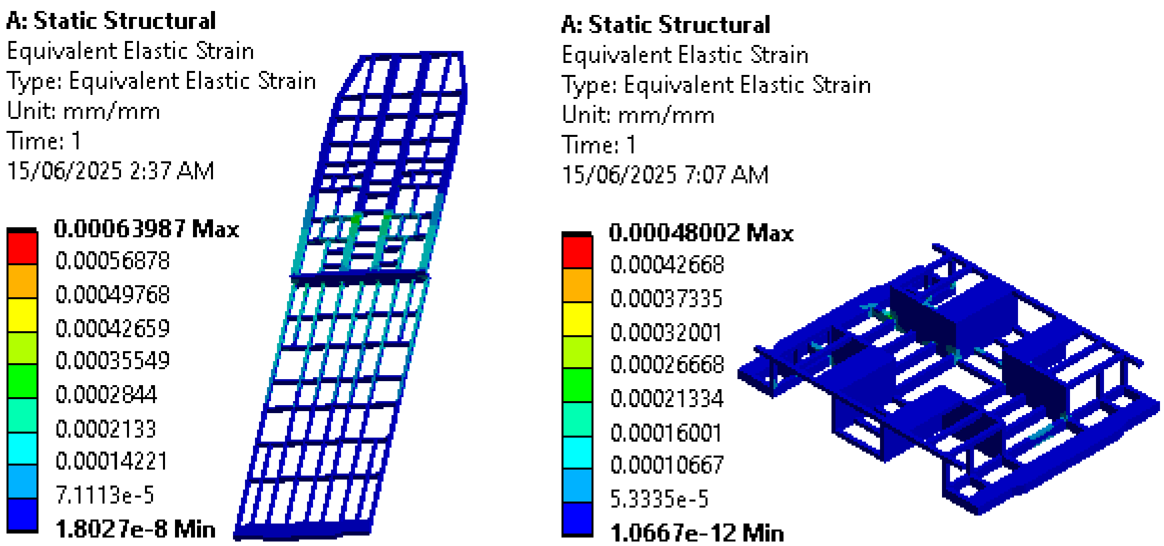

(a) (b)

Figure 4.17 Strain distribution of (a) MC1, and (b) TP underframe at 36 km/h

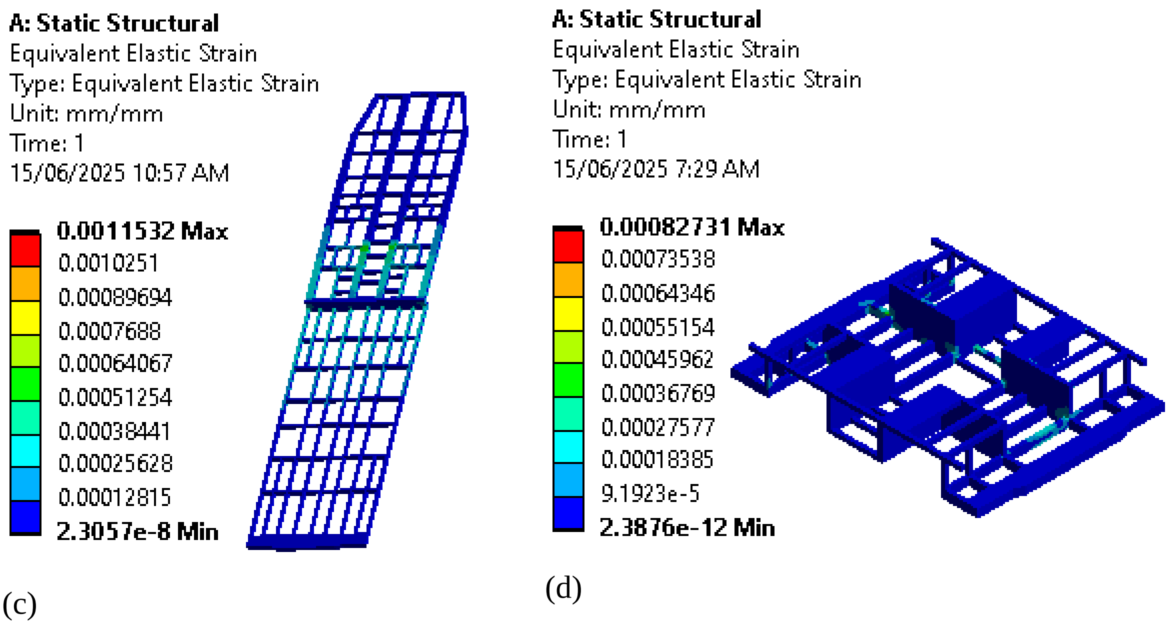

Figure 4.18 Strain distribution of (c) MC1, and (d) TP underframe at 50 km/h

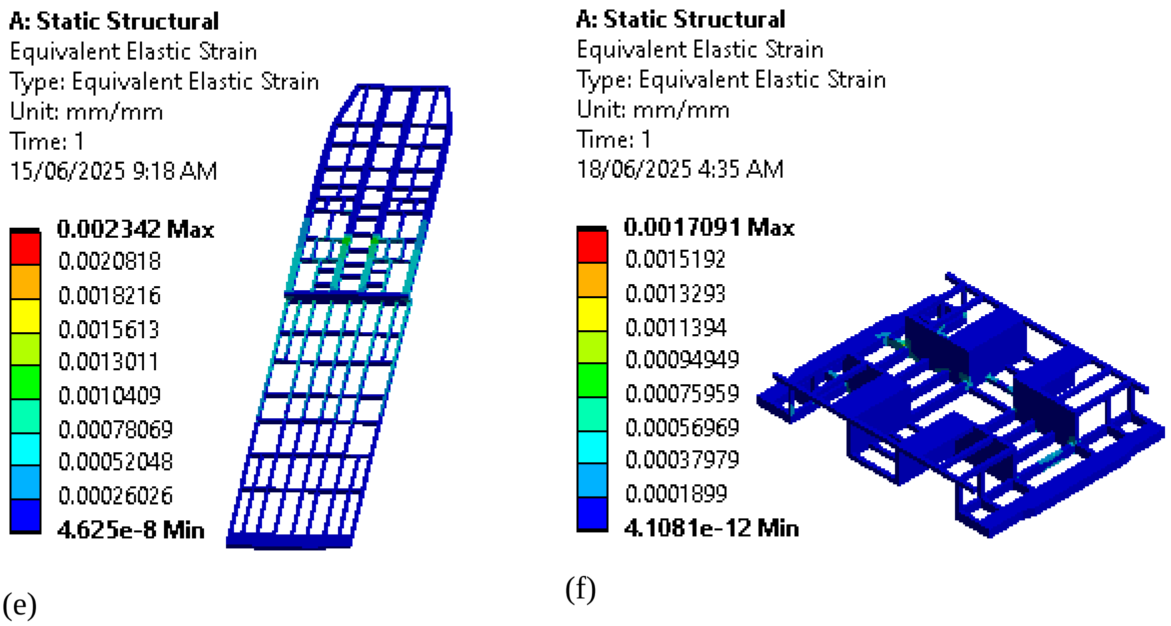

Figure 4.19 Strain distribution of (e) MC1, and (f) TP underframe at 70 km/h

Table 4.4 Maximum stress and Strain amplitude of MC and TP underframe

Speed(km/h)	MC underframe		TP underframe	
	Maximum stress (Mpa)	Strain amplitude (mm)	Maximum stress (Mpa)	Strain amplitude (mm)
36 km/h	108.63	3.199×10^{-4}	91.102	2.40×10^{-4}
50 km/h	195.75	5.77×10^{-4}	157.07	4.14×10^{-4}
70 km/h	394.9	1.17×10^{-3}	324.4	8.55×10^{-4}

Tables 4.6 and 4.7 present the simulated and calculated fatigue life results for the MC and TP underframes, respectively.

Table 4.5 Comparison of simulated and calculated life of MC underframe

Speed	Simulated life	Calculated life	Error (%)
36 km/h	$2.59*10^{9}$	$2.65*10^{9}$	2.3%
50 km/h	$2.45*10^{7}$	$2.30*10^{7}$	6.1%
70 km/h	$1.36*10^{5}$	$1.33*10^{5}$	2.2%

Table 4.6 Comparison of simulated and calculated life of TP underframe

Speed	Simulated life	Calculated life	Error (%)
36 km/h	$3.10*10^{10}$	$3.16*10^{10}$	1.9%
50 km/h	$1.12*10^{8}$	$1.20*10^{8}$	7.1%
70 km/h	$7.76*10^{5}$	$6.99*10^{5}$	9.9%

Comparison confirms that simulated fatigue life results are in good agreement with analytical SWT method predictions. This strong agreement confirms the validity of the developed numerical model for accurate prediction of railway underframe fatigue life under different operational conditions.

CHAPTER-5 CONCLUSION, RECOMMENDATION AND FUTURE WORK

5.1 Conclusion

This research examined the effects of track irregularities on the dynamic response and fatigue life of the LRVs underframe structure. The simulation results demonstrate that the motor car (MC) underframe experiences higher vertical and lateral accelerations than the trailer car (TP) underframe. This explains that the MC underframe is more prone to track irregularity excitations than the trailer car underframe.

Vertical accelerations are consistently higher than lateral accelerations in both MC and TP underframes. Thus, track irregularities have a stronger effect in the vertical direction. Moreover, as the operating speed increases, vertical and lateral accelerations also increase. This signifies the influence of track irregularities at higher speeds.

According to the FEM analysis, the underframes have the longest fatigue life at lower vehicle speeds (36 km/h) and the shortest fatigue life at maximum vehicle speeds (70 km/h). This indicates that the fatigue life of the underframe decreases significantly with increasing vehicle speed. This demonstrates that the effect of track irregularities is more significant at higher vehicle speeds, and thus decreases the fatigue life of the underframe.

Finally, the stress concentration nodes at the MC underframe are consistently located in the high-floor area. As a result, fatigue damage in the MC underframe is controlled by the high floor area, whereas the low-floor section is relatively unaffected.

5.2 Recommendations

Based on the findings of this research, the following recommendations are proposed for the longer service life of the underframe structure.

- This study indicates that the fatigue life of the underframe decreases significantly at higher vehicle speed (70 km/h) due to track irregularity excitations. To extend the service life of the underframe, light rail transit systems should establish a speed limit on the known irregular track sections.
- To minimize the effect of track irregularities on the underframe, light rail transit systems should perform regular maintenance and inspection on the railway track.

5.3 Future work

Further research could be conducted by incorporating additional parameters such as passenger loading and curved track sections, that might result in reduced underframe fatigue life. These parameters could be investigated in separate and combined effects in the dynamic behaviour and fatigue life of underframe in detail. This would provide a more thorough understanding of the effects encountered by light rail vehicles underframe for better design and maintenance procedures.

Reference

[1] O. Pietrzak and K. Pietrzak, "The role of railway in handling transport services of cities and agglomerations," *Transportation Research Procedia*, vol. 39, no. 2018, pp. 405–416, 2019, doi: 10.1016/j.trpro.2019.06.043.

[2] M. Ćwil, W. Bartnik, and S. Jarzębowski, "Railway vehicle energy efficiency as a key factor in creating sustainable transportation systems," *Energies (Basel).*, vol. 14, no. 16, pp. 1–13, 2021, doi: 10.3390/en14165211.

[3] A. Wondimu Tekolla, G. Segni Tulu, and A. Gebre Tarekegn, "Evaluating the Impact of Addis Ababa Light Rail Transit on Public Transit System, Its Efficiency and Eligibility for Transit Oriented Development (TOD)," *American Journal of Traffic and Transportation Engineering*, vol. 6, no. 6, p. 160, 2021, doi: 10.11648/j.ajtte.20210606.13.

[4] J. Sekasi and M. L. Martens, "Assessing the contributions of urban light rail transit to the sustainable development of addis ababa," *Sustainability (Switzerland)*, vol. 13, no. 10, pp. 1–22, 2021, doi: 10.3390/su13105667.

[5] D. da Fonseca-Soares, S. A. Eliziário, J. D. Galvincio, and A. F. Ramos-Ridao, "Greenhouse Gas Emissions in Railways: Systematic Review of Research Progress," *Buildings*, vol. 14, no. 2, pp. 1–22, 2024, doi: 10.3390/buildings14020539.

[6] T. Alade, J. Edelenbos, and A. Gianoli, "A Sustainable Approach to Innovation Adoption in Light-Rail Transport," 2020.

[7] H. De Bruijn and W. Veeneman, "Decision-making for light rail," *Transportation Research Part A*, vol. 43, no. 4, pp. 349–359, 2009, doi: 10.1016/j.tra.2008.11.003.

[8] A. Steimel, "Power-Electronics Issues of Modern Electric Railway Systems," no. May 2010, 2015, doi: 10.4316/aece.2010.02001.

[9] J. Fernández, M. A. Jiménez, J. M. Pradera, and S. Lafuente, "Application of the Substructuring Technique to the Stress Analysis of a Railcar Underframe Bolster," *ABAQUS Users' Conference*, pp. 1–14, 2003.

[10] C.-Q. Wang and F.-S. Li, "Vibration simulation of EMU carbody underframe considering rail short wave," pp. 627–632, 2017, doi: 10.1142/9789813208322_0070.

[11] B. W. Schlake, S. Todorovic, J. R. Edwards, J. M. Hart, N. Ahuja, and C. P. L. Barkan, "Machine vision condition monitoring of heavy-axle load railcar structural underframe components," *Proc. Inst. Mech. Eng. F J. Rail Rapid Transit*, vol. 224, no. 5, pp. 499–511, 2010, doi: 10.1243/09544097JRRT376.

[12] J. Chen, Y. Wu, X. He, L. Zhang, and S. Dong, "Suspension parameter design of underframe equipment considering series stiffness of shock absorber," *Advances in Mechanical Engineering*, vol. 12, no. 5, May 2020, doi: 10.1177/1687814020922647.

[13] E. Berhanu, “Overload effect on the life cycle of car body under frame steel structures for AALRT trains,” 2017.

[14] T. Karis, M. Berg, and S. Stichel, “Analysing the correlation between vehicle responses and track irregularities using dynamic simulations and measurements,” *Proc. Inst. Mech. Eng. F J. Rail Rapid Transit*, vol. 234, no. 2, pp. 170–182, 2020, doi: 10.1177/0954409719840450.

[15] D. Szoke and I. Zobory, “Analysis of bending stresses arising in the main beam of the underframe of a remotorised diesel locomotive under track irregularity excitation,” *Proceedings of the Mini Conference on Vehicle System Dynamics, Identification and Anomalies*, no. January 2008, pp. 239–248, 2008.

[16] L. Auersch, “Different Types of Continuous Track Irregularities as Sources of Train-Induced Ground Vibration and the Importance of the Random Variation of the Track Support,” *Applied Sciences (Switzerland)*, vol. 12, no. 3, pp. 15–17, 2022, doi: 10.3390/app12031463.

[17] T. Karis, *Correlation between Track Irregularities and Vehicle Dynamic Response Based on Measurements and Simulations*. 2018.

[18] J. F. Aceituno, R. Chamorro, S. Muñoz, and J. L. Escalona, “An alternative procedure to measure railroad track irregularities. Application to a scaled track,” *Measurement (Lond).*, vol. 137, pp. 417–427, 2019, doi: 10.1016/j.measurement.2019.01.025.

[19] L. Xin, L. Xu, J. Zhang, M. Pei, J. Mao, and D. Wang, “Research on characterization methods for track irregularities,” *Railway Engineering Science*, 2025, doi: 10.1007/s40534-024-00367-z.

[20] T. Karis, *Correlation between Track Irregularities and Vehicle Dynamic Response Based on Measurements and Simulations*.

[21] G. Bizimungu and C. Nkundineza, “Vibration Responses of the Railcar Under Rail Irregularities: Case of Addis Ababa Light Rail Transit,” *Journal of Vibration Engineering and Technologies*, vol. 11, no. 7, pp. 3535–3547, Oct. 2023, doi: 10.1007/s42417-022-00766-8.

[22] J. J. J. de Cisneros Fonfría, E. Olmeda, S. Sanz, M. Garrosa, and V. Díaz, “Failure analysis of a train coach underframe,” *Eng. Fail. Anal.*, vol. 156, no. October 2023, 2024, doi: 10.1016/j.engfailanal.2023.107756.

[23] Y. K. Al-Douri, P. Tretten, and R. Karim, “Improvement of railway performance: a study of Swedish railway infrastructure,” *Journal of Modern Transportation*, vol. 24, no. 1, pp. 22–37, 2016, doi: 10.1007/s40534-015-0092-0.

[24] C. Jonex, S. Aime Aliphones, and Z. Moges, “Railway Track Geometry Defects and Deterioration, a Literature Review,” *International Journal of Engineering and Applied Sciences (IJEAS)*, no. 9, pp. 2394–3661, 2022.

[25] J. Kanis, V. Zitrický, V. Hebelka, P. Lukáč, and M. Kubín, "Innovative diagnostics of the railway track superstructure," *Transportation Research Procedia*, vol. 53, no. 2019, pp. 138–145, 2021, doi: 10.1016/j.trpro.2021.02.017.

[26] S. Beskhyroun, L. D. Wegner, and B. F. Sparling, "Integral resonant control scheme for cancelling human-induced vibrations in light-weight pedestrian structures," *Struct. Control Health Monit.*, no. May 2011, p. n/a-n/a, 2011, doi: 10.1002/stc.

[27] L. Susmel, G. Meneghetti, and B. Atzori, "A simple and efficient reformulation of the classical Manson-Coffin curve to predict lifetime under multiaxial fatigue loading-part I: Plain materials," *J. Eng. Mater. Technol.*, vol. 131, no. 2, pp. 0210091–0210099, 2009, doi: 10.1115/1.3078300.

[28] A. Farkas, "Measurement of railway track geometry: A state-of-the-art review," *Periodica Polytechnica Transportation Engineering*, vol. 48, no. 1, pp. 76–88, 2019, doi: 10.3311/PPtr.14145.

[29] I. Y. Choi, J. H. Um, J. S. Lee, and H. H. Choi, "The influence of track irregularities on the running behavior of high-speed trains," *Proc. Inst. Mech. Eng. F J. Rail Rapid Transit*, vol. 227, no. 1, pp. 94–102, 2013, doi: 10.1177/0954409712455146.

[30] T. Karis, *Correlation between Track Irregularities and Vehicle Dynamic Response Based on Measurements and Simulations*. 2018.

[31] T. Karis, *Correlation between Track Irregularities and Vehicle Dynamic Response Based on Measurements and Simulations*.

[32] Q. Li, Z. Chen, Q. Hu, and L. Zhang, "Laser-Aided INS and Odometer Navigation System for Subway Track Irregularity Measurement," *Journal of Surveying Engineering*, vol. 143, no. 4, Nov. 2017, doi: 10.1061/(asce)su.1943-5428.0000236.

[33] T. Xin, P. Wang, and Y. Ding, "Effect of long-wavelength track irregularities on vehicle dynamic responses," *Shock and Vibration*, vol. 2019, 2019, doi: 10.1155/2019/4178065.

[34] C. F. Hung and W. L. Hsu, "Influence of long-wavelength track irregularities on the motion of a high-speed train," *Vehicle System Dynamics*, vol. 0, no. 0, pp. 1–18, 2017, doi: 10.1080/00423114.2017.1346261.

[35] A. Haigermoser, B. Luber, and J. Rauh, "Vehicle System Dynamics : International Journal of Vehicle Mechanics and Road and track irregularities : measurement , assessment and simulation," no. June, pp. 37–41, 2015, doi: 10.1080/00423114.2015.1037312.

[36] J. F. Aceituno, R. Chamorro, S. Muñoz, and J. L. Escalona, "An alternative procedure to measure railroad track irregularities. Application to a scaled track," *Measurement (Lond).*, vol. 137, pp. 417–427, 2019, doi: 10.1016/j.measurement.2019.01.025.

[37] E. M. Vinberg and A. H. Firdaus, "Railway Applications of Condition Monitoring," 2018, doi: 10.13140/RG.2.2.35912.62729.

[38] D. J. Thompson, G. Kouroussis, and E. Ntotsios, "Modelling, simulation and evaluation of ground vibration caused by rail vehicles*," *Vehicle System Dynamics*, vol. 57, no. 7, pp. 936–983, 2019, doi: 10.1080/00423114.2019.1602274.

[39] L. Niu, J. Liu, and Y. Zhou, "Track Irregularity Assessment in High-Speed Rail by Incorporating Carriage-Body Acceleration with Transfer Function," *Math. Probl. Eng.*, vol. 2020, 2020, doi: 10.1155/2020/8414531.

[40] S. Kaewunruen, "Monitoring structural deterioration of railway turnout systems via dynamic wheel/rail interaction," *Case Studies in Nondestructive Testing and Evaluation*, vol. 1, pp. 19–24, 2014, doi: 10.1016/j.csndt.2014.03.004.

[41] L. Wang, P. Wang, S. Quan, and R. Chen, "The effect of track alignment irregularity on wheel-rail contact geometry relationship in a turnout zone," *Journal of Modern Transportation*, vol. 20, no. 3, pp. 148–152, 2012, doi: 10.1007/bf03325792.

[42] L. Ling, Y. Deng, Q. Guan, and X. Jin, "Effect of track irregularities on the dynamic behavior of a tram vehicle," *Journal of Advances in Vehicle Engineering*, vol. 3, no. 1, pp. 29–39, 2017, doi: 10.1234/J73.

[43] J. Zeng, L. Wei, and P. Wu, "Safety evaluation for railway vehicles using an improved indirect measurement method of wheel–rail forces," *Journal of Modern Transportation*, vol. 24, no. 2, pp. 114–123, Jun. 2016, doi: 10.1007/s40534-016-0107-5.

[44] S. Lei, Y. Ge, and Q. Li, "Effect and its mechanism of spatial coherence of track irregularity on dynamic responses of railway vehicles," *Mech. Syst. Signal Process.*, vol. 145, 2020, doi: 10.1016/j.ymssp.2020.106957.

[45] T. Karis, M. Berg, and S. Stichel, "Analysing the correlation between vehicle responses and track irregularities using dynamic simulations and measurements," *Proc. Inst. Mech. Eng. F J. Rail Rapid Transit*, vol. 234, no. 2, pp. 170–182, 2020, doi: 10.1177/0954409719840450.

[46] N. Bosso, A. Bracciali, G. Megna, and N. Zampieri, "Effects of geometric track irregularities on vehicle dynamic behaviour when running through a turnout," *Vehicle System Dynamics*, vol. 61, no. 3, pp. 782–798, 2023, doi: 10.1080/00423114.2021.1957127.

[47] A. Miri, S. Mohammadzadeh, and H. Salek, "A finite element approach to develop track geometrical irregularity thresholds from the safety aspect," *Journal of Theoretical and Applied Mechanics (Poland)*, vol. 55, no. 2, pp. 695–705, 2017, doi: 10.15632/jtam-pl.55.2.695.

[48] X. Xiao, H. W. Xu, Y. Yang, P. Chen, and Q. Hu, "Analysis of the influence of track irregularity on high-speed train ride comfort," *Vehicle System Dynamics*, vol. 62, no. 7, pp. 1658–1685, 2024, doi: 10.1080/00423114.2023.2250888.

[49] W. Chang, X. Cai, Q. Wang, X. Tang, J. Sun, and F. Yang, “The Influence of Track Irregularity in Front of the Turnout on the Dynamic Performance of Vehicles,” *Applied Sciences (Switzerland)*, vol. 12, no. 9, 2022, doi: 10.3390/app12094169.

[50] C.-Q. Wang and F.-S. Li, “Vibration simulation of EMU carbody underframe considering rail short wave,” pp. 627–632, 2017, doi: 10.1142/9789813208322_0070.

[51] Y. Song, P. Wu, and L. Jia, “Study of the fatigue testing of a car body underframe for a high-speed train,” vol. 0, no. 0, pp. 1–12, 2016, doi: 10.1177/0954409715618425.

[52] Y. Song, P. Wu, and L. Jia, “Study of the fatigue testing of a car body underframe for a high-speed train,” Aug. 01, 2016, *SAGE Publications Ltd*. doi: 10.1177/0954409715618425.

[53] H. K. Jun, H. S. Jung, D. H. Lee, J. W. Seo, and S. J. Kwon, “Fatigue crack evaluation on the underframe of EMU carbody,” *Procedia Eng.*, vol. 2, no. 1, pp. 893–900, 2010, doi: 10.1016/j.proeng.2010.03.096.

[54] W. Lu *et al.*, “Corrosion fatigue crack propagation behavior of A7N01P-T4 aluminum alloy welded joints from high-speed train underframe after 1.8 million km operation,” *Materials and Corrosion*, vol. 72, no. 5, pp. 879–887, 2021, doi: 10.1002/maco.202012123.

[55] B. W. Schlake, S. Todorovic, J. R. Edwards, J. M. Hart, N. Ahuja, and C. P. L. Barkan, “Machine vision condition monitoring of heavy-axle load railcar structural underframe components,” *Proc. Inst. Mech. Eng. F J. Rail Rapid Transit*, vol. 224, no. 5, pp. 499–511, 2010, doi: 10.1243/09544097JRRT376.

[56] Y. Song, P. Wu, and L. Jia, “Study of the Equivalent Load on the Local Component of the Car Body,” no. Icmce, pp. 341–351, 2014.

[57] J. M. Hart, B. Schlake, N. M. Ave, and J. R. Edwards, “RTDF2009-18043,” 2017.

[58] B. W. Schlake, S. Todorovic, J. R. Edwards, J. M. Hart, N. Ahuja, and C. P. L. Barkan, “Machine vision condition monitoring of heavy-axle load railcar structural underframe components,” *Proc. Inst. Mech. Eng. F J. Rail Rapid Transit*, vol. 224, no. 5, pp. 499–511, 2010, doi: 10.1243/09544097JRRT376.

[59] S. E. Michael and C. A. B. Perlman, “Side Structure Integrity Research for Passenger Rail Equipment.”

[60] F. Railroad Administration, “Crash Energy Management: One- and Two-Car Passenger Rail Impact Tests.”

[61] R. A. Smith, “Railway fatigue failures: An overview of a long standing problem,” *Materwiss. Werksttech.*, vol. 36, no. 11, pp. 697–705, Nov. 2005, doi: 10.1002/mawe.200500939.

[62] M. M. Mohammed, "Fundamental Drivers of Metal Fatigue Failure and Performance," *Multidisciplinary Materials Chronicles*, vol. 1, no. 1, pp. 49–61, 2024, doi: 10.62184/mmc.jmmc110020245.

[63] R. Xiu, M. Spiryagin, Q. Wu, S. Yang, and Y. Liu, "Fatigue life assessment methods for railway vehicle bogie frames," Oct. 01, 2020, *Elsevier Ltd*. doi: 10.1016/j.engfailanal.2020.104725.

[64] B. Miao, W. Zhang, J. Zhang, and D. Jin, "Evaluation of Railway Vehicle Car Body Fatigue Life and Durability using a Multi-disciplinary Analysis Method," *International Journal of Vehicle Structures & Systems*, vol. 1, no. 4, Nov. 2009, doi: 10.4273/ijvss.1.4.20.

[65] Y. Lu *et al.*, "Analysis of the dynamic response and fatigue reliability of a full-scale carbody of a high-speed train," *Proc. Inst. Mech. Eng. F J. Rail Rapid Transit*, vol. 232, no. 7, pp. 2006–2023, Aug. 2018, doi: 10.1177/0954409718757295.

[66] Y. Lu, W. Bi, X. Zhang, J. Zeng, T. Chen, and P. Wu, "Calculation method of dynamic loads spectrum and effects on fatigue damage of a full-scale carbody for high-speed trains," *Vehicle System Dynamics*, vol. 58, no. 7, pp. 1037–1056, Jul. 2020, doi: 10.1080/00423114.2019.1605080.

[67] B. R. Miao, W. H. Zhang, G. H. Huang, S. C. Wu, and Y. X. Zhao, "Research of high speed train carbody structure vibration behaviors and structure fatigue strength characteristic technology," in *Advanced Materials Research*, 2012, pp. 256–261. doi: 10.4028/www.scientific.net/AMR.544.256.

[68] B. Miao, W. Zhang, J. Zhang, and D. Jin, "Evaluation of Railway Vehicle Car Body Fatigue Life and Durability using a Multi-disciplinary Analysis Method," *International Journal of Vehicle Structures & Systems*, vol. 1, no. 4, Nov. 2009, doi: 10.4273/ijvss.1.4.20.

[69] A. Momhur, Y. X. Zhao, W. Q. Li, Y. Z. Sun, and X. L. Zou, "Flexible-Rigid Wheelset Introduced Dynamic Effects due to Wheel Tread Flat," *Shock and Vibration*, vol. 2021, 2021, doi: 10.1155/2021/5537286.

[70] "Maintenance Manual".

[71] A. Obsie, M. Woldeamanuel, and B. Woldetensae, "Service Quality of Addis Ababa Light Rail Transit: Passengers' Views and Perspectives," *Urban Rail Transit*, vol. 6, no. 4, pp. 231–243, Dec. 2020, doi: 10.1007/s40864-020-00135-2.

[72] A. Momhur, Y. X. Zhao, W. Q. Li, Y. Z. Sun, and X. L. Zou, "Flexible-Rigid Wheelset Introduced Dynamic Effects due to Wheel Tread Flat," *Shock and Vibration*, vol. 2021, 2021, doi: 10.1155/2021/5537286.

[73] B. R. Miao, W. H. Zhang, G. H. Huang, S. C. Wu, and Y. X. Zhao, "Research of high speed train carbody structure vibration behaviors and structure fatigue strength

characteristic technology," in *Advanced Materials Research*, 2012, pp. 256–261. doi: 10.4028/www.scientific.net/AMR.544.256.

[74] A. Gupta, P. Deka, and N. Debnath, "MODELLING AND ANALYSIS OF AN IRREGULAR RAILWAY TRACK SYSTEM FOR COMPUTATION OF CRITICAL VELOCITY FOR LIMITING VERTICAL ACCELERATION," *Stavební obzor - Civil Engineering Journal*, vol. 27, no. 1, Apr. 2018, doi: 10.14311/cej.2018.01.0012.

[75] O. Javaid and D. H. Choi, "Effect of track irregularities on the response of two-way railway tracks," *Applied Sciences (Switzerland)*, vol. 10, no. 1, Jan. 2020, doi: 10.3390/app10010011.

[76] K. Cui and D. Lv, "Experiment and simulation research of the ground-borne vibration for a high-speed train," *Journal of Vibroengineering*, vol. 18, no. 3, pp. 1783–1797, 2016, doi: 10.21595/jve.2016.16673.

[77] T. Xin, P. Wang, and Y. Ding, "Effect of long-wavelength track irregularities on vehicle dynamic responses," *Shock and Vibration*, vol. 2019, 2019, doi: 10.1155/2019/4178065.

[78] W. Li *et al.*, "Dynamic Responses of Train-Symmetry-Bridge System Considering Concrete Creep and the Creep-Induced Track Irregularity," *Symmetry (Basel).*, vol. 15, no. 10, Oct. 2023, doi: 10.3390/sym15101846.

[79] I. Y. Choi, J. H. Um, J. S. Lee, and H. H. Choi, "The influence of track irregularities on the running behavior of high-speed trains," *Proc. Inst. Mech. Eng. F J. Rail Rapid Transit*, vol. 227, no. 1, pp. 94–102, 2013, doi: 10.1177/0954409712455146.

[80] J. Hu, L. Xie, R. Zhang, and W. Yin, "Failure analysis of a crack on a train bolster," *Eng. Fail. Anal.*, vol. 97, pp. 32–42, Mar. 2019, doi: 10.1016/j.engfailanal.2018.12.010.

[81] Y. Hu, Z. Hu, and S. Cao, "Theoretical study on Manson-Coffin equation for physically short cracks and lifetime prediction," *Sci. China Technol. Sci.*, vol. 55, no. 1, pp. 34–42, 2012, doi: 10.1007/s11431-011-4581-z.

[82] T. Pertoll, M. Leitner, C. Buzzi, and L. Boronkai, "Strain-Based Assessment to Evaluate Damage Caused by Deep Rolling," *Materials*, vol. 17, no. 9, May 2024, doi: 10.3390/ma17092163.

Appendices

Appendix A. Underframe Hotspot Nodes

Hotspot nodes of MC underframe at 70 km/h

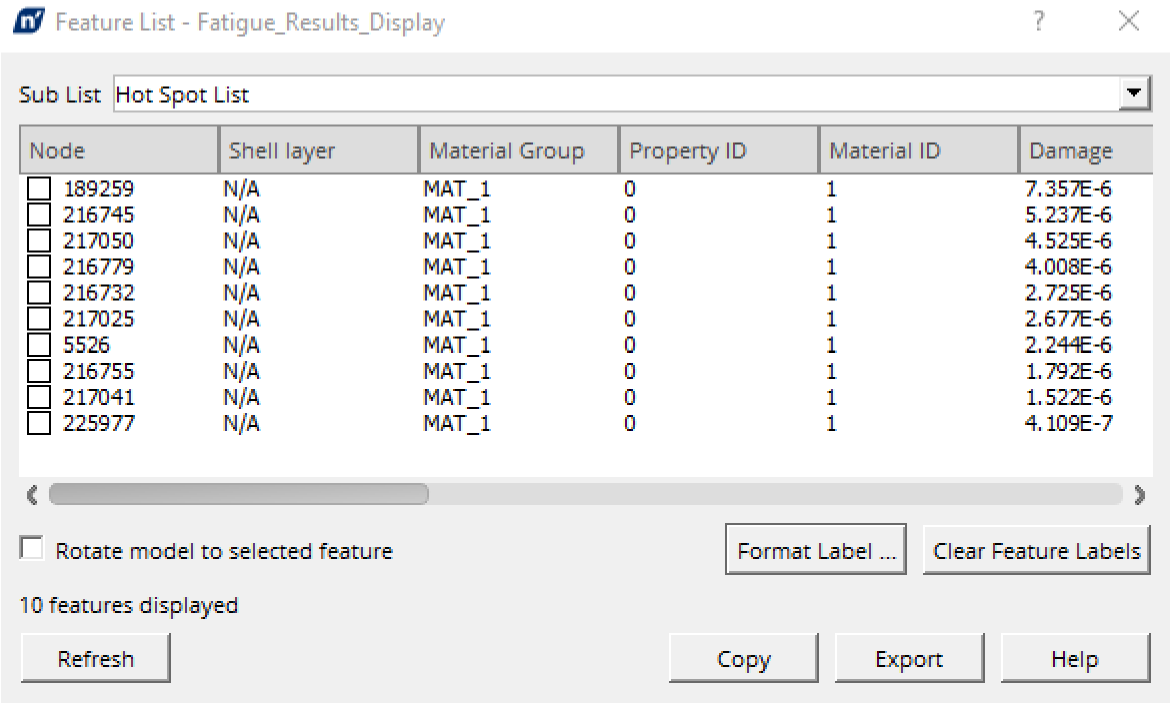

Node	Shell layer	Material Group	Property ID	Material ID	Damage
189259	N/A	MAT_1	0	1	7.357E-6
216745	N/A	MAT_1	0	1	5.237E-6
217050	N/A	MAT_1	0	1	4.525E-6
216779	N/A	MAT_1	0	1	4.008E-6
216732	N/A	MAT_1	0	1	2.725E-6
217025	N/A	MAT_1	0	1	2.677E-6
5526	N/A	MAT_1	0	1	2.244E-6
216755	N/A	MAT_1	0	1	1.792E-6
217041	N/A	MAT_1	0	1	1.522E-6
225977	N/A	MAT_1	0	1	4.109E-7

Hotspot nodes of MC underframe at 70 km/h

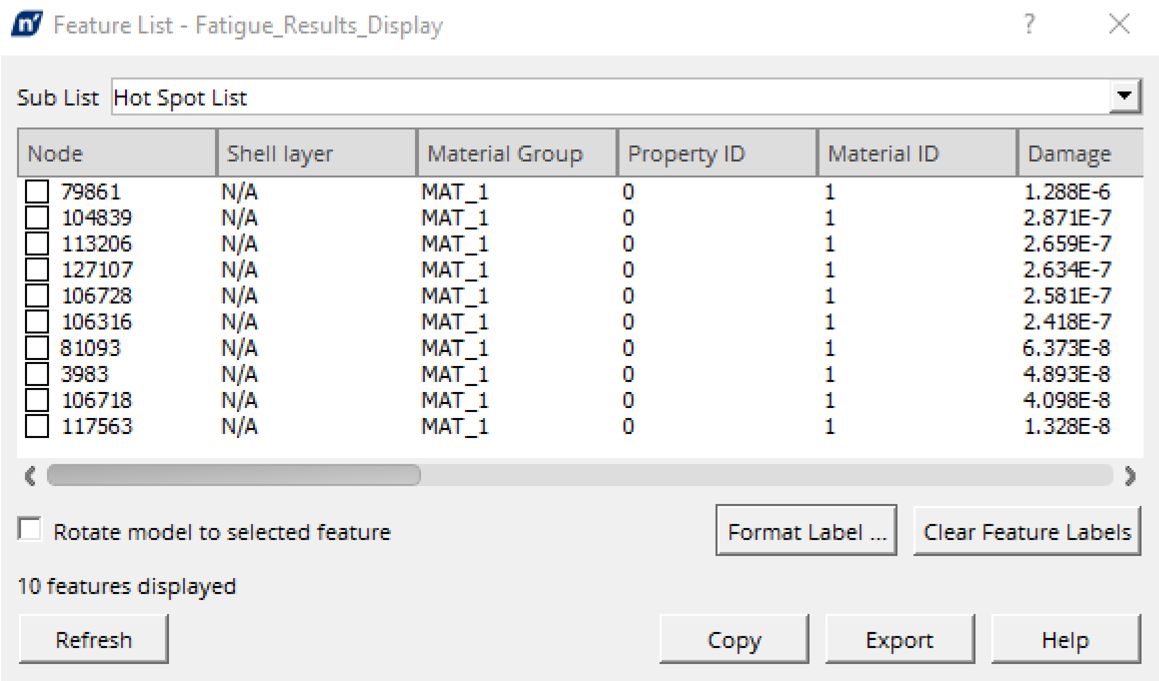

Node	Shell layer	Material Group	Property ID	Material ID	Damage
79861	N/A	MAT_1	0	1	1.288E-6
104839	N/A	MAT_1	0	1	2.871E-7
113206	N/A	MAT_1	0	1	2.659E-7
127107	N/A	MAT_1	0	1	2.634E-7
106728	N/A	MAT_1	0	1	2.581E-7
106316	N/A	MAT_1	0	1	2.418E-7
81093	N/A	MAT_1	0	1	6.373E-8
3983	N/A	MAT_1	0	1	4.893E-8
106718	N/A	MAT_1	0	1	4.098E-8
117563	N/A	MAT_1	0	1	1.328E-8

Appendix B. Phyton code for fatigue life calculation

Python code for fatigue life calculation of MC underframe at 70 km/h.

```
import numpy as np
from scipy.optimize import fsolve

# Material and loading parameters
E = 204000  # Young's modulus in MPa (204 GPa)
sigma_f_prime = 930  # Fatigue strength coefficient in MPa
epsilon_f_prime = 0.298  # Fatigue ductility coefficient
b = -0.106  # Fatigue strength exponent
c = -0.49  # Fatigue ductility exponent
sigma_max = 394.9  # Maximum stress in MPa
epsilon_a = 1.17e-3  # Strain amplitude (calculated)

# SWT parameter (left-hand side of the equation)
SWT = sigma_max * epsilon_a

# Define the SWT equation as a function of 2N_f (reversals)
def swt_equation(two_Nf):
    term1 = (sigma_f_prime**2 / E) * (two_Nf)**(2 * b)  # Elastic term
    term2 = sigma_f_prime * epsilon_f_prime * (two_Nf)**(b + c)  # Plastic term
    return SWT - (term1 + term2)  # Residual for root finding

# Initial guess for 2N_f (adjusted for low-cycle fatigue)
initial_guess = 1e4

# Solve for 2N_f using fsolve with increased tolerance
two_Nf_solution, = fsolve(swt_equation, initial_guess, xtol=1e-8)

# Convert to cycles to failure (N_f)
Nf = two_Nf_solution / 2

# Print N_f in scientific notation
print(f"N_f = {Nf:.2e} cycles")
```

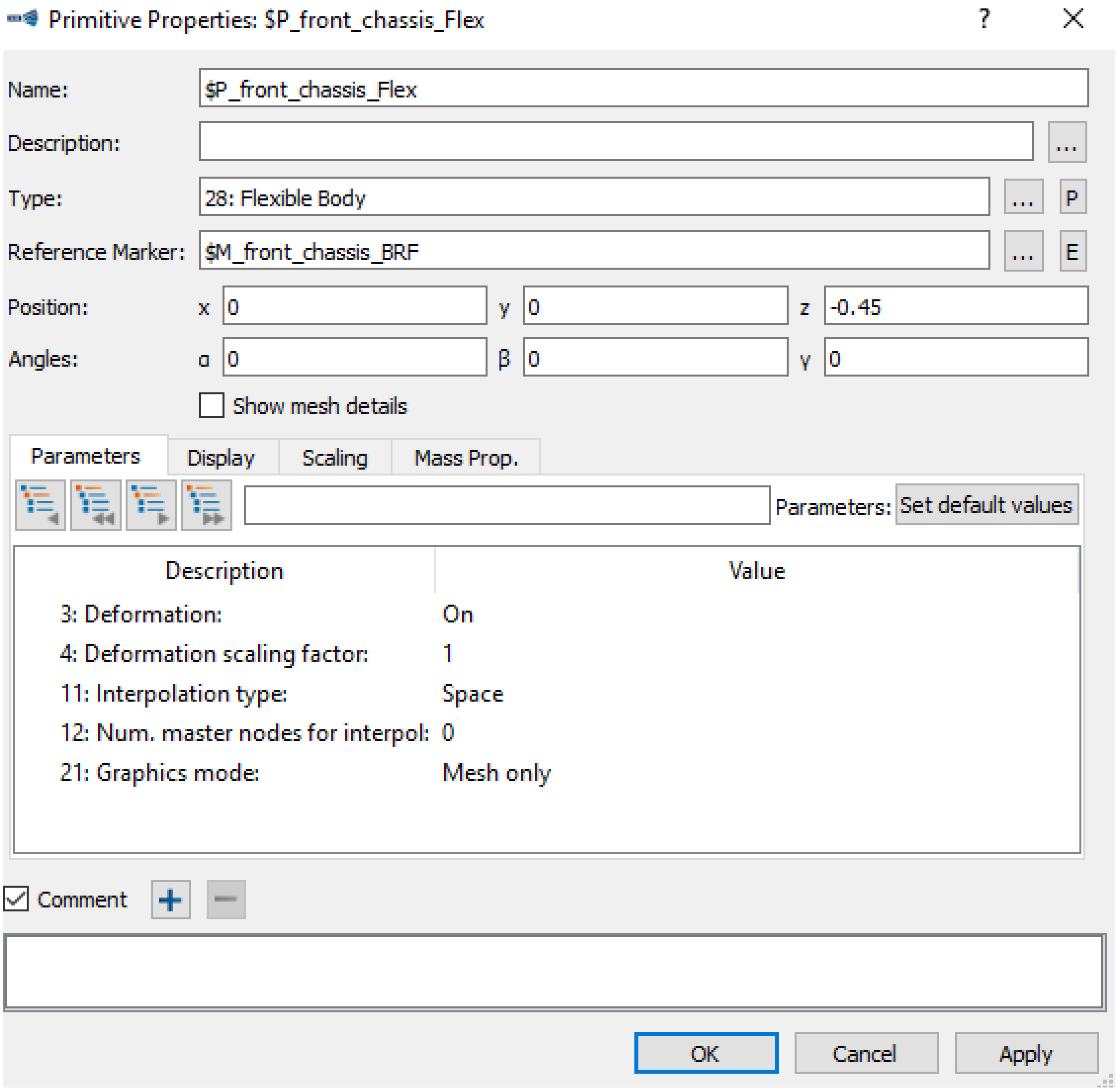
Primitive Properties: $P_front_chassis_Flex
Name:
$P_front_chassis_Flex
Description:
Type:
28: Flexible Body
P
Reference Marker:
$M_front_chassis_BRF
E
Position:
x 0
y 0
z -0.45
Angles:
α 0
β 0
γ 0
Show mesh details
Parameters
Display
Scaling
Mass Prop.
Parameters:
Set default values
Description
Value
3: Deformation:
On
4: Deformation scaling factor:
1
11: Interpolation type:
Space
12: Num. master nodes for interpol:
0
21: Graphics mode:
Mesh only
Comment
OK
Cancel
Apply